

**MODELING OPTICAL PROPERTIES OF THIN FILM CU(IN,GA)SE₂ SOLAR
CELLS USING SPECTROSCOPIC ELLIPSOMETRY**

by

Scott H. Stephens

A thesis submitted to the faculty of the University of Delaware in the partial fulfillment
of the requirements for the degree of Master of Science in Physics

Winter 2006

© 2006 Scott H. Stephens
All Rights Reserved

UMI Number: 1432297



UMI Microform 1432297

Copyright 2006 by ProQuest Information and Learning Company.
All rights reserved. This microform edition is protected against
unauthorized copying under Title 17, United States Code.

ProQuest Information and Learning Company
300 North Zeeb Road
P.O. Box 1346
Ann Arbor, MI 48106-1346

**MODELING OPTICAL PROPERTIES OF THIN FILM CU(IN,GA)SE₂ SOLAR
CELLS USING SPECTROSCOPIC ELLIPSOMETRY**

by

Scott H. Stephens

Approved: _____
Robert W. Birkmire, Ph.D.
Professor in charge of thesis on behalf of the Advisory Committee

Approved: _____
George Hadjipanayis, Ph.D.
Chair of the Department of Physics and Astronomy

Approved: _____
Tom Apple, Ph.D.
Dean of the College of Arts and Sciences

Approved: _____
Conrado M. Gempesaw II, Ph.D.
Vice Provost for Academic and International Programs

ACKNOWLEDGMENTS

I would like to thank William Shafarman for his help, support, and patience with my work, Robert Birkmire for keeping me on track towards a completing a degree, Puther Paulson for teaching me all about VASE, Brian McCandless for helping me with XRD runs, and Steven Hegedus for answering all of my renewable energy related questions. I would also like to extend my thanks to everyone at IEC for always being approachable and accommodating. Lastly I want to thank Bhupender, Fazle, Jonathan, Michael, Som, and Takahiro; not only for getting me through the past two years but also for making it a very enjoyable experience.

TABLE OF CONTENTS

LIST OF FIGURES	vi
LIST OF TABLES	ix
ABSTRACT	x

Chapter

1	INTRODUCTION AND BACKGROUND	1
2	BACKGROUND	4
	2.1 Ellipsometry	4
	2.2 Cu(In,Ga)Se ₂	5
	2.3 CdS	7
3	ELLIPSOMETRY ANALYSIS	8
	3.1 Instrument	8
	3.2 Optical Response of Materials and Layered Structures	12
	3.3 Measurement	19
	3.4 Data Modeling	22
4	EXPERIMENTAL	36
	4.1 Deposition	36
	4.2 Sample Preparation	38
	4.3 VASE Measurement	41
	4.4 Non-VASE Analysis	43
5	RESULTS	45
	5.1 Mo	45
	5.2 MoSe ₂	49
	5.3 Cu(In,Ga)Se ₂	54
	5.4 CdS	65

6	CONCLUSION AND FUTURE WORK	71
6.1	Conclusion	71
6.1.1	Mo.....	71
6.1.2	MoSe ₂	71
6.1.3	Cu(In,Ga)Se ₂	72
6.1.4	CdS.....	72
6.1.5	Ellipsometry.....	73
6.2	Future Work	74
	BIBLIOGRAPHY	75

LIST OF FIGURES

3.1	Standard optical elements of an ellipsometer shown for reflection measurement	9
3.2	Variable Angle Spectroscopic Ellipsometer with AutoRetarder	10
3.3	Dielectric and optical constants for a lorentz oscillator with $\omega_0 = 3\text{eV}$ and $\gamma=.25\text{eV}$	14
3.4	The parallel component of a wave reflecting at an interface less than (a), at (b), and greater than (c) the Brewster angle. The reflected beam is simply the re-radiation of dipole oscillators within the medium and is illustrated as their projection in the direction of the reflected ray.....	16
3.5	Light reflecting from a sample composed of a single film on a substrate. The first three reflections are shown and expressed in terms of their Fresnel coefficients and phase change.....	17
3.6	Brewster scan for an etched CuGaInSe ₂ (33923.21) sample measured at 1 and 3.5 eV. This data shows that the greatest Ψ sensitivity will be achieved at angle between 70° and just over 75°. CuGaInSe ₂ data for this work was measured at angles of 65°, 70°, and 75° to ensure sufficient variation in measured data and because data taken above 75° often yields insufficient intensity.....	21
3.7	Flowchart of the standard iterative VASE data analysis procedure	24
3.8	Simplified single parameter MSE fitting using Newton’s method and path of steepest decent	28
3.9	Sharp Δ flips of a CuGaInSe ₂ sample with a bandgap of approximately 1.1 eV (33843.21). The three lines correspond to incident angles of 65°, 70°, and 75° which span the pseudo-Brewster angle	30

3.10	Point-By-Point generated data for k of a MoSe_2 sample which is reproduced by linearly summing three lorentz oscillators which are consistent with the Kramers-Kronig relations of eq. (3.18). Notice the unphysical low-energy ripples in the point-by-point data are removed using the oscillator model.....	33
4.1	Schematic diagram of a typical Cu(In,Ga)Se_2 sample as prepared by IEC	36
4.2	Cu(In,Ga)Se_2 sample preparation before (a) and after (b) using peeling method.....	40
4.3	Optical models used to model samples prepared by etching (a) or peeling (b) methods	42
5.1	Mo optical constants obtained from VASE models. Variations in the modeled surface roughness significantly influence n . The effect of Na diffusion can be noted by comparing the optical constants of samples prepared on Soda-Lime with 7059 glass	48
5.2	Differences between a general oscillator model and a point-by-point fit of a selenized MoSe_2 sample. These slight differences indicate that the Mo data in the optical model is slightly inaccurate and that this error could propagate to the MoSe_2 fit	50
5.3	Ψ measured first under Ar flow immediately after peeling and then again after 14 hour exposure to air at room temperature.....	51
5.4	MoSe_2 optical constants obtained from VASE analysis on peeled and selenized samples. The close agreement for the two peeled samples suggests that the optical properties of the MoSe_2 layer in high efficiency devices are consistently different from films prepared by selenization.....	53
5.5	RMS roughness of Cu(In,Ga)Se_2 films etched under a range of Br_2 concentrations and times. For consistency, etch times were based upon the concentration so that all films underwent approximately equal changes in thickness. The change in film thickness for all samples shown was greater than the initial z-range roughness	55
5.6	AFM images taken before and after applying a standard etch of 0.03 M Br_2 for 60 seconds. The etched RMS is approximately 10nm which satisfies the optically smooth criterion well beyond 4.6 eV	56

5.7	Three general oscillators used to model the bandgap of the Cu(In,Ga)Se ₂ layer. The sharp onset of these transitions was described using asymmetric Gaussian broadened polynomial superposition oscillators. The linear superposition of the three oscillators is represented by the dashed line and the solid line is the dielectric function produced by the point-by-point fit.....	60
5.8	Measured and generated values of Ψ for an etched Cu(In,Ga)Se ₂ sample. Disagreement between the model and data occurs around the bandgap region (1.0 -1.3 eV) shown more clearly in the inset image. A final MSE of 4.7 was obtained for this fit.....	61
5.9	Differences in the refractive index n for peeled and etched samples. The samples were from runs 33843 (top) and 33845 (bottom).....	63
5.10	Differences in the extinction coefficient k for peeled and etched samples. The samples were from runs 33843 (top) and 33845 (bottom).....	64
5.11	GIXRD spectrums (offset for comparison) for a CdS/Mo/7059 sample after successive heat treatments of 20 minutes at 400° C (HT 1) and 30 minutes at 500 ° C (HT 2) in argon. Data is shown using a three point binomial smooth and $\lambda = 1.5405\text{\AA}$	66
5.12	Dielectric constant of CdS modeled using two general oscillators. Linear summation of these two oscillators (dotted line) is in good agreement with the point-by-point data (solid line)	68
5.13	Optical constants of CBD CdS and an etched CdTe sample. Extinction coefficients are shown over a narrowed range to resolve bandgap behavior more clearly. The annealed sample is HT 2 from Figure 5.11	69

LIST OF TABLES

- 5.1 Cell performance with different Cu(In,Ga)Se₂ etches and heat treatment. Samples marked with * indicate results shown are after a 2 minute heat-treat of the completed device at 200°C in air. Other samples did not improve with this treatment.....58
- 5.2 MoSe₂ thickness for Cu(In,Ga)Se₂/MoSe₂/Mo samples with successively thinner Cu(In,Ga)Se₂ surface layers as fit by the VASE. Surface roughnesses were also fit except in the case of sample 33844.31b which was limited to a maximum value of 50Å to ensure physicality59

ABSTRACT

In this research, the optical properties of Cu(In,Ga)Se₂ thin film solar cells were modeled using variable angle spectroscopic ellipsometry and compared against established optical data from bulk materials. Mo, MoSe₂, Cu(In,Ga)Se₂ and CdS films were measured individually as the devices were formed layer by layer. Optical data, thickness, surface roughness, and the methodology of preparing and effectively modeling samples have been determined. Diffusion of Na from the Soda Lime glass substrate is evident in the optical constants of the Mo layer. The optical constants of the MoSe₂ layer were found to be dependent upon the deposition conditions. The bandgap of the CdS layer was higher when deposited on Cu(In,Ga)Se₂ surfaces than when deposited on Mo. This implies that greater lattice strain is present in the CdS layer of solar cell devices than that of CdS films previously measured in CdS/Mo structures.

Chapter 1

MOTIVATION

In 2004, world installation of solar photovoltaic panels (PV) increased 62% to 927 megawatts of peak power [1]. Increasing efficiency, decreasing price, and economics of scale have sustained 20 to 25% growth for the past 20 years. While this consistent growth is impressive (especially throughout periods of inexpensive fossil fuels), PV still today represents less than one tenth of one percent of all electrical generation. Furthermore, much of the growth seen in PV installations thus far has been due to government subsidies and early adopters. To maintain this growth, studies suggest that the price per peak watt must continue to fall [2]. Thus far, progress has been made through increased efficiency and with volume production. Standard crystalline silicon panels have been in production for over three decades, however, and efficiency improvements have slowed. While manufacturing costs have fallen to almost $\$4/W_{\text{peak}}$, there remain significant costs involved with the energy intensive purification of bulk silicon. Finally, a recent shortage of silicon feedstock has affected completed module prices [3] indicating the significant base material costs involved with this design. Analysts speculate that PV modules must reach a target price of less than $\$2/W_{\text{peak}}$ before becoming a significant energy producer and that PV based upon energy and material intensive silicon may not be able to meet this price point.

A promising alternative is the production of thin film PV with layers that are 500 to 1000 times thinner than conventional silicon modules. Cu(In,Ga)Se₂-based thin film solar cells currently offer the highest efficiency as well as excellent stability and potentially low cost manufacturing. Much of the progress realized with this material has been driven experimentally rather than being motivated by an understanding of fundamental properties. PV remains the most significant application for Cu(In,Ga)Se₂ [4] and further improvements in performance will necessitate a clear understanding of the intrinsic material and device physics of this quaternary material.

An effective means of investigating Cu(In,Ga)Se₂-based PV is to study the optical properties of films prepared for high performance solar cells. The optical response of a sample can be probed directly with absorption or quantum efficiency measurements. Alternatively, an indirect approach known as spectroscopic ellipsometry can be used to model a layered thin film structure. With this method, optical constants and thicknesses of each layer can be determined. By analyzing optical constants across an energy spectrum information regarding the films physical and band structure can be worked out.

Optical data on many materials can be found in literature or in handbooks [5]. However this data is often obtained from bulk materials or from films prepared on different substrates and with different deposition conditions. These discrepancies can lead to significant changes in the optical response of a film and studying the absorbing layer's bandgap or overall device efficiency can be more difficult. By measuring the optical constants of films that are prepared as high efficiency devices and comparing this

information with prior optical data, information regarding the physics of the films and devices can be better understood.

This project examines the optical properties of layers found in Cu(In,Ga)Se₂ cells that are prepared as high efficiency PV devices. Mo, MoSe₂, Cu(In,Ga)Se₂ and CdS films were measured individually as the devices were formed layer by layer. Optical data as well as the methodology of preparing and effectively modeling samples is presented. This data is analyzed and, whenever possible, correlations between optical behavior and physical properties are made.

Chapter 2

BACKGROUND

2.1 Ellipsometry

Paul Drude first reported the use of spectroscopic ellipsometry (SE) in 1886 while studying Sb_2S_3 crystals [6]. Observing a time dependent change in the polarization of reflected light and correctly attributing this change to the growth of a thin oxide layer on the freshly cleaved surface motivated Drude to formulate the general equations of ellipsometry. While his equations were exact, computational limitations at the time necessitated the use of approximations. After Drude's initial studies, the field of ellipsometry was largely neglected for nearly 75 years. During this time some progress was made using the reflectance of unpolarized light to measure thickness. Although algorithmically simple, this approach assumed wavelength independent diffraction and relied upon some initial knowledge of the material's optical properties. Philipp [7] extended the usefulness of reflectometry by obtaining optical constants of bulk material using the Kramers-Kronig relation to calculate the phase argument of the Fresnel equation. The quality of these measurements however is limited both in theory and in practice. The Kramers-Kronig relations require knowledge of spectral reflectance from zero to infinity and thus, with limited data, small series termination errors are induced in the calculation of n and k . Additionally, baseline intensity drifts of the incident beam and

difficulties collecting 100% of the reflected beam complicate the measurement. Lastly, because reflectance measurements yield optical data based on direct calculations, the approach cannot correct for over layers or surface roughness.

While reflectometry remains an efficient method of measuring thickness of well-characterized films, advancements in both digital processing power as well as rotating analyzer prisms [8] have vastly improved the usefulness of the ellipsometer. Originally, measurements were performed at one or a few individual wavelengths using a laser or a filtered arc lamp but continued improvements of fast monochrometers have allowed precise data to be taken from the infrared to ultraviolet (1700-270nm). The *spectroscopic* ellipsometer yields continuous optical data of materials and allows multi-layer and depth profiling analysis to be performed. Ellipsometry accuracy has been further enhanced with the use of variable angle spectroscopic ellipsometry (VASE) which has the advantage of collecting more data by measuring light at multiple angles of incidence. The data measured is used to justify or refine a working model of the material and thus collecting data at different angle allows a more substantial comparison between generated and measured data. Today, ellipsometry has become the preferred non-destructive optical technique for obtaining the dispersion parameters of multi-layered structures, measurement of very thin films ($<50\text{\AA}$), and analysis of microstructural information.

3.2 Cu(In,Ga)Se₂

The optical properties of the Cu(In,Ga)Se₂ quaternary chalcopyrite structure have been examined broadly. The dielectric tensor components for single CuInSe₂ and

CuGaSe₂ crystals have been measured [9, 10] resolving the slight anisotropy of the crystal. However, for these studies, precise ellipsometry data was only obtained over a limited range [9] (1.2-5.3 eV) above the bandgap or at a fixed incidence angle [10] ($\phi=65^\circ$). Additionally, because this data was obtained for bulk crystals, the results may differ from thin film measurements. Further optical studies [11] were carried out on well characterized polycrystalline Cu(In,Ga)Se₂ ingots prepared by direct fusion of the constituent elements. Because the crystals were randomly oriented and smaller than the probing wavelengths, no anisotropic effects were measured. Again however, this data was taken on bulk samples.

Hermann et al. [12] performed the first reported ellipsometry analysis of Cu(In,Ga)Se₂ solar cells prepared as high efficiency devices. The Cu(In,Ga)Se₂ layer was deposited by both sputtering and physical vapor techniques on Mo substrates. However, difficulties modeling the bandgap region were encountered in this study due to significant surface roughness. Recently a detailed examination of high performance Cu(In,Ga)Se₂ films by Paulson et al. [13] examined the optical effects as a function of relative Ga incorporation. Samples were prepared by peeling the film away from the Mo and measuring the backside. This approach ensured the Cu(In,Ga)Se₂ was smooth enough to obtain precise optical data.

In this work, an alternative approach of smoothing the Cu(In,Ga)Se₂ surface by chemical etching was pursued. Data modeling of the Cu(In,Ga)Se₂ layer closely followed the methods used by Paulson, but because the samples weren't peeled, differences in the layers below the Cu(In,Ga)Se₂ (sublayers) had to be accounted for.

With this approach, the differences between the optical response of peeled and etched Cu(In,Ga)Se₂ films was studied.

3.3 CdS

The Cu(In,Ga)Se₂ layer is typically followed by a CdS film to fabricate a solar cell. This window layer can be deposited with various techniques including vapor-phase [14, 15], spray pyrolysis [16], electrodeposition, and sputtering. For this work, a chemical bath deposition (CBD) was employed. This technique is common with high efficiency cells and was the preparation method used by Rakhshani et al. [17] for his analysis of CdS films. However, Rakhshani used only absorption measurements to establish the optical response of the film and like others, prepared his films on glass substrates. Further, Rakhshani notes that lattice strain is dependent upon the film's thickness, indicating that the choice of substrate can affect the optical response of the film. Because the CdS films prepared in high efficiency devices are thin (~50nm) and epitaxial effects such as strain may significantly affect the optical properties of the film, samples for this work were prepared directly on the Cu(In,Ga)Se₂ layer. Additionally, CdS films were bath deposited on other substrates and the optical responses were compared to note the substrate's effect.

Chapter 3

ELLIPSOMETRY ANALYSIS

Two misconceptions exist regarding the analysis of ellipsometry data [18]. The first is that due to the indirect measurement and modeling techniques, successful analysis is more art than science. The theory and practice of obtaining physical and optical information, however, is purely analytical and will be developed in this chapter. After this understanding is established, the second fallacy, that ellipsometry is an “all-powerful” approach that can be easily applied to unknown samples, will be addressed. In practice, it is best to be maximally informed prior to modeling a sample. The second half of this chapter will discuss this general process. Mathematical details primarily follow after [19] and except where otherwise cited, general principles of ellipsometry are taken from [18, 20].

3.1 Instrument

An effective method of characterizing semiconductors is by studying their optical properties (i.e. the interaction of the material with light). Ellipsometry is one such technique in which polarized light is used to evaluate the dipole response or density of a solid. The basic ellipsometer is composed of a series of optical elements as shown in Figure 3.1.

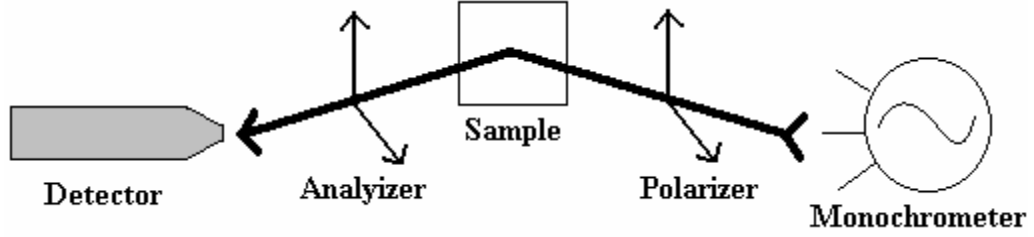


Figure 3.1: Standard optical elements of an ellipsometer shown for reflection measurements.

Monochromatic light is linearly polarized and then reflected off the surface or transmitted through a sample. The phase difference of the parallel and perpendicular components changes as the beam interacts with the sample interfaces and in general becomes elliptically polarized. This elliptical light is then measured with a rotating polarizing element (analyzer) to determine the light's component amplitudes and phase difference. Thus, for each wavelength and angle, two measurements are made. One is the change in phase difference

$$\Delta = \delta_1 - \delta_2 \quad (3.1)$$

where δ_1 and δ_2 are the phase differences between components before and after reflection respectively. The other is the ratio of amplitudes

$$\Psi = \tan^{-1} \left(\frac{|R^{\parallel}|}{|R^{\perp}|} \right) \quad (3.2)$$

with $|R^{\parallel}|$ and $|R^{\perp}|$ are the real components of Fresnel's reflection coefficients. These parameters are often related using the fundamental equation of ellipsometry.

$$\tan \Psi e^{i\Delta} = \frac{R^{\parallel}}{R^{\perp}} \quad (3.3)$$

The advantage of these ratio quantities is that their measurement is not susceptible to intensity drift, beam spreading, or imperfections in a reference sample. The two measured quantities are also somewhat complimentary; Δ is sensitive to film thicknesses less than 100Å while Ψ can be used to precisely determine the dispersion of thicker films. Taken together they are able to quantify many subtle optical effects introduced by the various layers of the sample.

All ellipsometry measurements for this work were performed with a Variable Angle Spectroscopic Ellipsometry (VASE) from J. A. Woollam Co. shown in Figure 3.2.

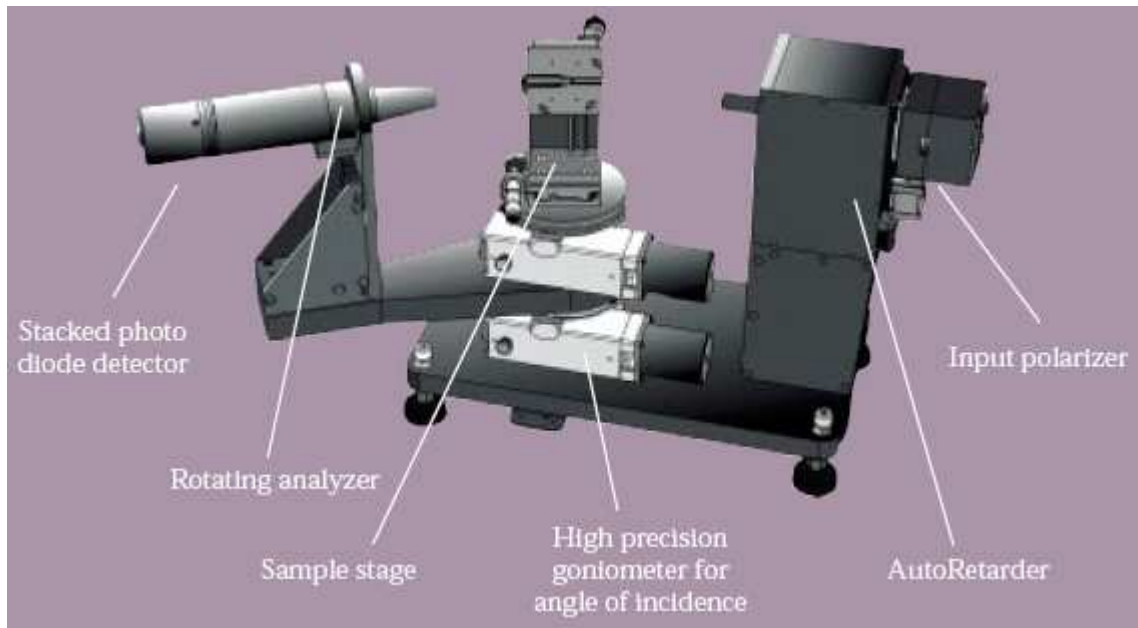


Figure 3.2: Variable Angle Spectroscopic Ellipsometer with AutoRetarder from J. A. Woollam [21].

Not shown are the 75W HS-190 monochromator (optimized for speed, wavelength accuracy, and light throughput) and the fiber optic cable with a spectral range from 240-1700nm. Data is recorded in a lit room and so a mechanical chopper is used to ensure synchronous intensity detection. The vertical sample stage is designed to allow transmission as well as reflection ellipsometry to be performed. The VASE uses a rotating analyzer and a fixed angle input polarizer. The advantage of this configuration, as opposed to a rotating polarizer setup, is that the monochromator beam doesn't need to be perfectly unpolarized. However, the difficulty with a rotating analyzer is that the detector must not exhibit any polarization sensitivity. Also, the phase quantity that is actually measured is $\cos \Delta$, so any rotating element setup will exhibit large uncertainty when Δ is close to 0° or 180° . To overcome this limitation, the VASE instrument shown in Figure 3.2 utilizes a compensator called an AutoRetarder which achromatically induces a 90° change in Δ . Thus by recording both normal and retarded measurements, consistent high precision can be obtained over the full spectrum. Additionally, the signal to noise measurement of $\tan \Psi$ is improved if the polarizer is close to the value of Ψ so the VASE adjusts the polarizing angle to previously measured value of Ψ before recording each measurement, a process known as polarizer tracking. The rotating analyzer VASE equipped with an AutoRetarder offers precision and reproducibility in its measurement of Ψ and Δ . However such control is of little value without proper understanding of how these parameters relate to optical properties and physical quantities of the sample.

3.2 Optical Response of Materials and Layered Structures

The most productive approach to understanding the propagation of light through a solid is to use the classical model of dipole oscillators. In this model, a material is composed of frequency dependent dipole oscillators that can be correlated with lattice, molecular, or atomic interactions. At optical frequencies the dominant dipole response is from oscillations of bound electrons and can be expressed classically using the Lorentz Oscillator model

$$m_0 \frac{d^2 x}{dt^2} + m_0 \gamma \frac{dx}{dt} + m_0 \omega_0^2 x = -e\mathcal{E} \quad (3.4)$$

where m_0 is the electron mass, γ is the damping rate, and ω_0 is the natural frequency response of the electron with charge e . The terms on the left represent the acceleration, damping, and Hook's restoring force respectively and the term on the right, \mathcal{E} , is the incident EM wave or driving force. The displacement from equilibrium $x(t)$ is found by expressing the electric field as a monochromatic plane wave $\mathcal{E}(t) = \mathcal{E}_0 e^{-i\omega t}$ and finding solutions of the form $x(t) = X_0 e^{i\omega t}$ (where \mathcal{E}_0 and X_0 are complex). Using the dipole equation, the induced macroscopic polarization is given by

$$P_{resonant} = \frac{Ne^2}{m_0} \frac{\mathcal{E}}{(\omega_0^2 - \omega^2 - i\gamma\omega)} \quad (3.5)$$

where m_0 is the electron mass and N is the atomic density. The electric displacement

$\vec{D} = \epsilon_0 \vec{\mathcal{E}} + \vec{P}_{background} + \vec{P}_{resonant}$ can be used to solve for the relative permittivity or dielectric

constant ϵ_r of an isotropic material with the relationship $\vec{D} = \epsilon_0 \epsilon_r \vec{\mathcal{E}}$, which gives

$$\varepsilon_r(\omega) = 1 + \chi + \frac{Ne_2}{\varepsilon_0 m_0} \frac{1}{(\omega_0^2 - \omega^2 - i\gamma\omega)} \quad (3.6)$$

where χ is the electric susceptibility. This complex quantity is often separated into its real and imaginary terms $\varepsilon_r = \varepsilon_1 + i\varepsilon_2$.

$$\varepsilon_1(\omega) = 1 + \chi + \frac{Ne^2}{\varepsilon_0 m_0} \frac{\omega_0^2 - \omega^2}{(\omega_0^2 - \omega^2)^2 + (\gamma\omega)^2} \quad (3.7)$$

$$\varepsilon_2(\omega) = \frac{Ne^2}{\varepsilon_0 m_0} \frac{\gamma\omega}{(\omega_0^2 - \omega^2)^2 + (\gamma\omega)^2}$$

It should be noted that these terms are called “constants” for historical reasons but in fact are functions strongly dependent upon ω in the vicinity of ω_0 . Additionally, for most semiconductors, multiple resonances exist for a material. In this case, $\varepsilon_r(\omega)$ is written as a linear summation of oscillators each with their own characteristic resonance. The dielectric constants can be thought of as expressions of what happens to the material when probed with light. Alternatively, the *optical* constants, $N = n + ik$, explain what happens to the light as it interacts with the material. The relation between the complex quantities, $\varepsilon_r = N^2$, can be used to express the real and imaginary components of the optical constants.

$$n = \sqrt{\frac{1}{2} \left[(\varepsilon_1^2 + \varepsilon_2^2)^{1/2} + \varepsilon_1 \right]} \quad (3.8)$$

$$k = \sqrt{\frac{1}{2} \left[(\varepsilon_1^2 + \varepsilon_2^2)^{1/2} - \varepsilon_1 \right]}$$

Conceptually, n is inversely proportional to the velocity of light in the material, and k is related to the absorption α through the expression $\alpha = \frac{4\pi k}{\lambda}$. The functions of the four “constants” are plotted for a lorentzian oscillator with $\omega_0 = 3\text{eV}$ and $\gamma=0.25\text{eV}$ in the following figure.

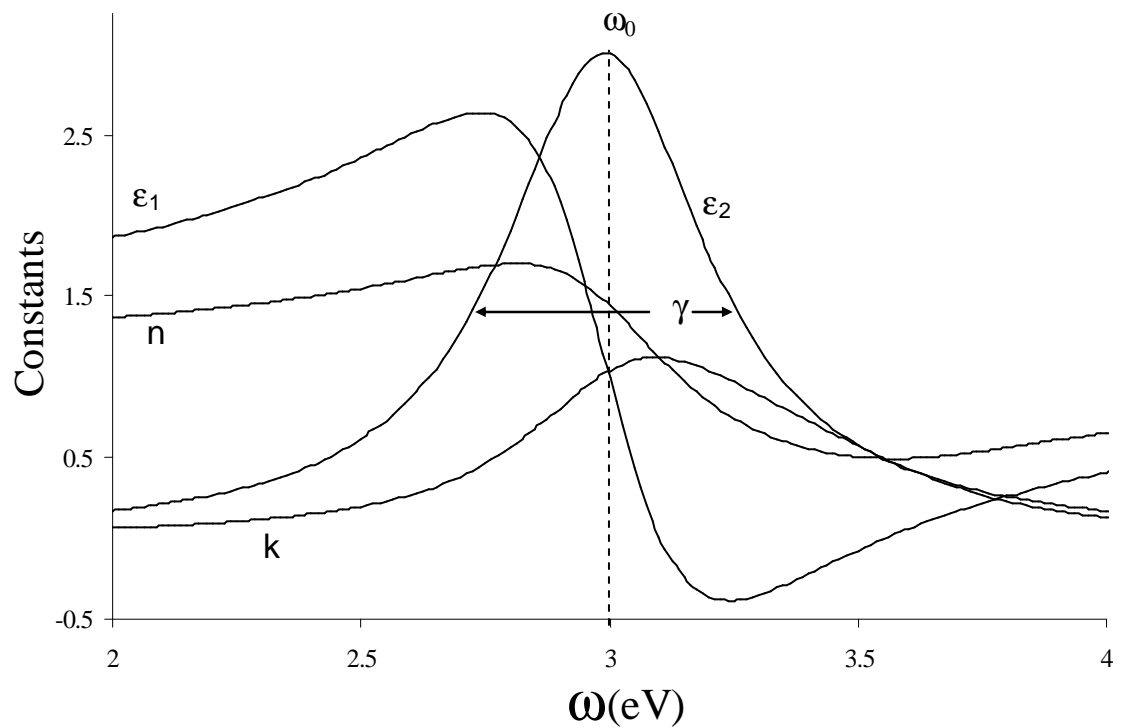


Figure 3.3: Dielectric and optical constants for a Lorentz oscillator with $\omega_0 = 3\text{eV}$ and $\gamma = 0.25\text{eV}$.

When the frequency of incident light matches the natural resonance of an electron in the material, very large oscillations will be induced and result in an excitation of that electron

and absorption of the light. Off resonance the absorption is quickly reduced but the damping quantity γ remains significant in ϵ_1 and n . Thus, dispersion can be observed where there is very little absorption of light.

While ϵ_1 and ϵ_2 are more representative of the dipole oscillator model, n and k are referred to more often because they directly describe the behavior of light which is the measured quantity. Therefore, it is important to fully understand how n and k affect the measured ellipsometry quantities Ψ and Δ .

Upon first consideration, one might expect that for an isotropic sample the phase shift and amplitude attenuation would be the same for both components of light. If this were the case, measurements of Ψ and Δ would always yield values of 45° and 0° respectively and would be useless. While it is true that isotropic materials don't affect Ψ and Δ as the light propagates through them, these quantities are affected at the interface of layers. The most familiar example of this is observed for reflection from a single interface.

Light projected onto a surface can be represented in components that are parallel and perpendicular to the plane of incidence. Upon reflection the parallel component experiences greater attenuation than the perpendicular component because the dipole axis makes a small angle with the reflected ray. At a certain geometry, the transmitted and reflected beams form a right angle and the dipole oscillations in the medium will not reflect any E_{\parallel} component of the beam. This angle is known as the polarizing or Brewster angle because only E_{\perp} is reflected and yields a Ψ value of zero.

The other ellipsometry quantity, Δ , is also dependent upon the Brewster angle as illustrated in Figure 3.4.

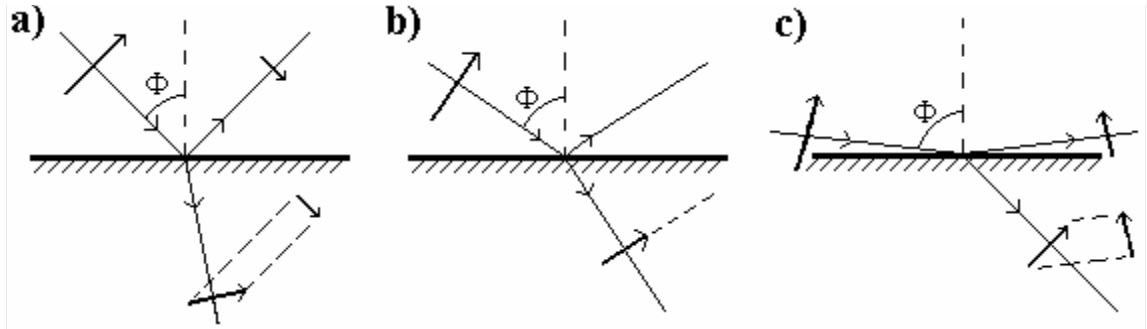


Figure 3.4: The parallel component of a wave reflecting at an interface less than (a), at (b), and greater than (c) the Brewster angle. The reflected beam is simply the re-radiation of dipole oscillators within the medium and is illustrated as their projection in the direction of the reflected ray.

For Figure 3.4a, the phase of the parallel component's reflected beam is flipped 180° while the perpendicular component remains unchanged. However, as the angle of incidence is increased beyond the Brewster angle, Figure 3.4c, the phase is unchanged by reflection and $\Delta = 0^\circ$.

Using Maxwell's wave equation, boundary conditions can be employed to analytically study the behavior of light at the interface of materials. Snell's law, a result of phase matching at the interface, yields the transmission of light from material one to material two.

$$N_1 \sin \phi_1 = N_2 \sin \phi_2 \quad (3.9)$$

where ϕ_i is the angle from normal incidence with which the light meets the interface. A second boundary condition is the continuity of the wave's \vec{E} and \vec{B} field components

across the boundary. Solving for this condition yields the fraction of light that is transmitted and reflected for components parallel and perpendicular to the plane of incidence. These amplitude ratios are known as the Fresnel coefficients.

$$\begin{aligned}
 t_{1,2}^{\parallel} &= \frac{2N_1 \cos \phi_1}{N_2 \cos \phi_1 + N_1 \cos \phi_2} & t_{1,2}^{\perp} &= \frac{2N_1 \cos \phi_1}{N_1 \cos \phi_1 + N_2 \cos \phi_2} \\
 r_{1,2}^{\parallel} &= \frac{N_2 \cos \phi_1 - N_1 \cos \phi_2}{N_2 \cos \phi_1 + N_1 \cos \phi_2} & r_{1,2}^{\perp} &= \frac{N_1 \cos \phi_1 - N_2 \cos \phi_2}{N_1 \cos \phi_1 + N_2 \cos \phi_2}
 \end{aligned}
 \tag{3.10}$$

For samples with a single air/bulk interface, Fresnel's and Snell's equations adequately explain the behavior of light. Often however, the more complicated case of samples with a deposited layer and thus more than one interface is encountered. As shown in Figure 3.5, a fraction of light is reflected back from the second interface and a fraction of this light is transmitted back out of the sample.

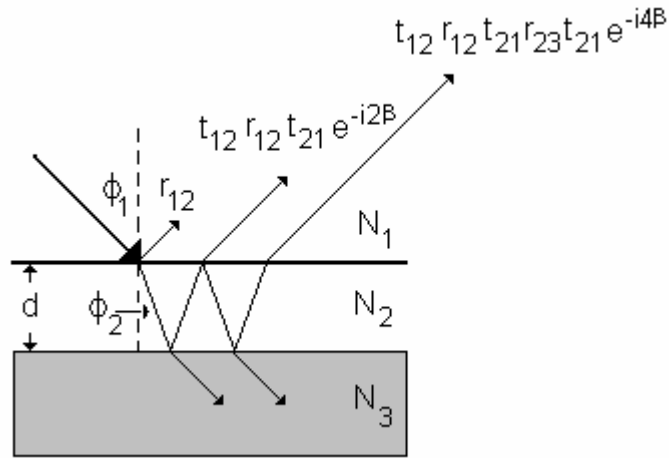


Figure 3.5: Light reflecting from a sample composed of a single film on a substrate. The first three reflections are shown and expressed in terms of their Fresnel coefficients and phase change.

To calculate the *total* reflection or transmission the amplitude and phase of these reflections must be taken into account. The change in phase (phase= δ , not Δ) that occurs as the light passes through the film is known as the film phase thickness [22]

$$\beta = 2\pi \left(\frac{d}{\lambda_2} \right) N_2 \cos \phi_2 \quad (3.11)$$

where d is the layer thickness and λ_2 is the light wavelength within layer two. This effective phase thickness must be considered to account for interference from the successive reflections. The total reflection can be calculated by summing the reflection terms in a geometrical expansion. Written in component form the total coefficients are given by the following equations.

$$\begin{aligned} T^{\parallel} &= \frac{t_{1,2}^{\parallel} t_{2,3}^{\parallel} e^{-i\beta}}{1 + r_{1,2}^{\parallel} r_{2,3}^{\parallel} e^{-i2\beta}} & T^{\perp} &= \frac{t_{1,2}^{\perp} t_{2,3}^{\perp} e^{-i\beta}}{1 + r_{1,2}^{\perp} r_{2,3}^{\perp} e^{-i2\beta}} \\ R^{\parallel} &= \frac{r_{1,2}^{\parallel} + r_{2,3}^{\parallel} e^{-i2\beta}}{1 + r_{1,2}^{\parallel} r_{2,3}^{\parallel} e^{-i2\beta}} & R^{\perp} &= \frac{r_{1,2}^{\perp} + r_{2,3}^{\perp} e^{-i2\beta}}{1 + r_{1,2}^{\perp} r_{2,3}^{\perp} e^{-i2\beta}} \end{aligned} \quad (3.12)$$

For samples with more than one deposited film, a recursive approach is used. If a sample has two films on a substrate, the total reflection is first calculated without regard to the top film. This value then becomes $r_{2,3}$ and the calculation can be performed as before.

The actual multi-layer formalism used by the VASE software (WVASE32) [18] is based on “characteristic matrices” according to Jones or Muller matrix formalism. These matrices describe the change in field components across an interface. The advantage of this approach is largely mathematical, not conceptual, but the important result is that if

the optical constants are known for each layer, Ψ and Δ can be easily computed directly for either reflection or transmission ellipsometry.

The complicated combination of rays, each having a different amplitude and phase, generates values of Ψ and Δ that vary substantially with angle and wavelength. It is this variation that allows the ellipsometry parameters to be useful in characterizing a sample. Thus, while ellipsometry is fundamentally a probe of dipole density, it is the interface separation and index variations that allow the technique to work. A clear understanding of the polarizing effects of layered structures is of use in nearly all aspects of ellipsometry, beginning with the technical process of data collection.

3.3 Measurement

The first question to be addressed when considering ellipsometry analysis is what type of samples can be effectively studied with this approach. The first criterion is that the probing light be able to reach all the layers of interest. If a layer is determined to be optically thick over the full spectrum of incident light then it is the effective substrate and nothing below it will be measurable. For partially transparent films, thickness measurements are limited to scales within two orders of magnitude of the wavelength of probing light. Also, because the illuminated spot on the sample is approximately three-square millimeters in area, thickness non-uniformity must be considered and should not exceed 10% over this area. Finally, although Ψ and Δ are ratio measurements and thus not sensitive to light scattering, the detector must receive sufficient intensity. As a rule of thumb, the surface of a sample should be “optically smooth” with features less than 10%

of the probe beam wavelength. If these conditions are met a fairly straightforward procedure is followed for data collection.

As with many optical instruments the VASE requires that the polarizing elements (see Figures 3.1 and 3.2) be calibrated but because Ψ and Δ are ratio measurements, drifts in beam intensity or detector response and do not need to be considered. Using a standardized sample, a series of measurements is performed where the polarizer and analyzer are adjusted until their exact angular positions are established. After this automated calibration, the sample to be measured is suctioned to the vertical stage and the X, Y, and Z axes are adjusted so that the reflected beam from the sample's surface is directed properly towards the detector. At this point, if the general sample type has been studied before, then the standard measurement settings can be applied. If the sample is unique from previous experience, then further setup is required to determine the ideal measurement parameters.

The VASE measures Ψ and Δ as a function of angle and wavelength to indirectly determine physical or optical features of a sample. The effectiveness of this approach is limited to the sensitivity Ψ and Δ have to these features. Therefore, it is important to select a range of angles and spectrum of wavelengths that will maximize this sensitivity. Looking at eq. (3.2) and Figure 3.4 it is clear that at the Brewster angle the parallel component of light is maximally absorbed into the sample and thus provides the best contrast and variation of Ψ . However because the Brewster angle is itself a function of wavelength, a spectroscopic ellipsometer most effectively measures Ψ in the *pseudo*-Brewster angle range. To determine this range, Ψ is measured as the incidence angle is

scanned for two wavelengths that bound the measurable spectrum. The standard scans were performed at 1 and 3.5 eV with angles of 50° to 85° and a step size of 1°. The minimum values of Ψ as shown in Figure 3.6 and the value at which $\Delta=90^\circ$ (Figure 3.4b) for these two bounding wavelengths give the range of the pseudo-Brewster angle.

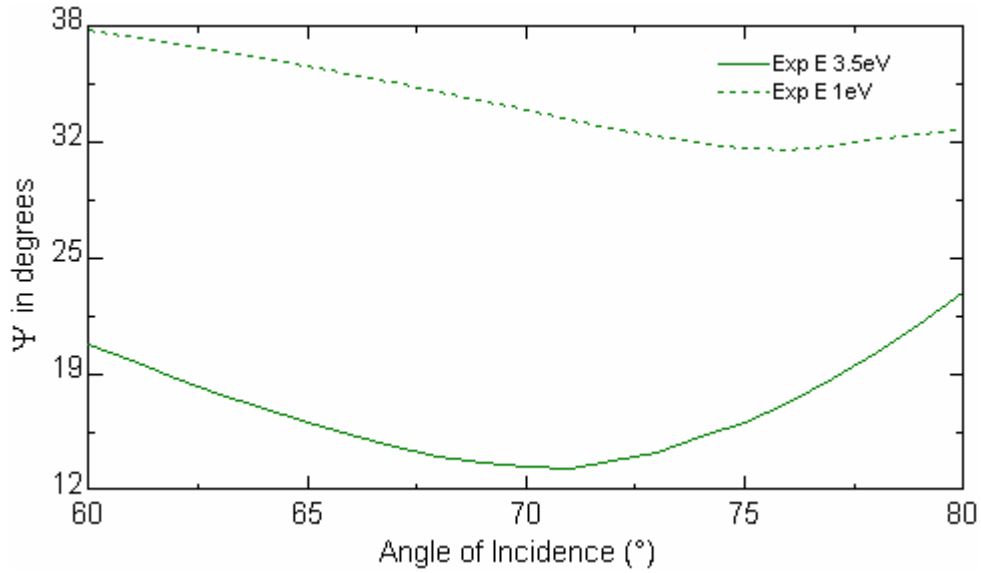


Figure 3.6: Brewster scan for an etched Cu(Ga,In)Se₂ (33923.21) sample measured at 1 and 3.5 eV. This data shows that the greatest Ψ sensitivity will be achieved at angle between 70° and just over 75°. Cu(Ga,In)Se₂ data for this work was measured at angles of 65°, 70°, and 75° to ensure sufficient variation in measured data and because data taken above 75° often yields insufficient intensity.

After selecting measurement angles, an estimation of the spectral range and resolution used to probe the material must be made. If a sample's bandgap or regions of high dispersion are known then a smaller monochromator step may be used at these

wavelengths. Typically, the full spectrum allowed by the fiber optic cabling is measured at least with a large step so that optical constants can be obtained over this full range.

The last step before data is collected is to select measurement options such as the use of the AutoRetarder or Polarizer Tracking. Also, if the sample is expected to be depolarizing [23] (introducing circular polarization or incoherent scattering) or anisotropic then these characteristics can be accounted with additional measurements. Lastly, to ensure consistent sensitivity over the full spectrum, the number of analyzer rotations per measurement can be dynamically adjusted as the data is taken. A higher number of rotations (one measurement per rotation) will statistically reduce (\sqrt{N} / N) the noise in Ψ and Δ . The intensity of reflectance will vary with wavelength and angle, so by dynamically adjusting the rotations per measurement all data can be fit with significant weighting. Considering these options carefully is important because the quality and completeness of measured data is directly related to its usefulness for ellipsometric model analysis.

3.4 Data Modeling

Extracting optical and physical information about a sample from Ψ and Δ is known as the “inverse problem”. In section 3.2 the direct method of calculating Ψ and Δ given the optical properties of a layered sample was discussed, however no such direct approach exists when working the opposite direction (except for the simplest case of a bulk sample with no surface layers). The basic problem is that of uniqueness; structures with significantly different layers could conceivably give rise to identical

values of Ψ and Δ . Therefore the only approach is to create a detailed mathematical model and attempt to recreate the measured data by varying model parameters such as optical constants and thickness of films. Two disadvantages of this approach are that it is computationally intensive and when a fit is achieved the physicality of the results must be evaluated. The main advantage of this modeling approach is that any property of the sample that alters Ψ and Δ (and can be accurately integrated into the model) can be indirectly measured. These properties that affect measured ellipsometry data include optical constants, layer thicknesses, interface compositions, crystallinity, thickness uniformity, and backside reflection. Uniqueness constraints prevent the fitting of all these parameters simultaneously and so an iterative modeling procedure is followed where the most optically significant properties are adjusted first and later the more subtle parameters are fit. This general approach is illustrated schematically in Figure (3.7).

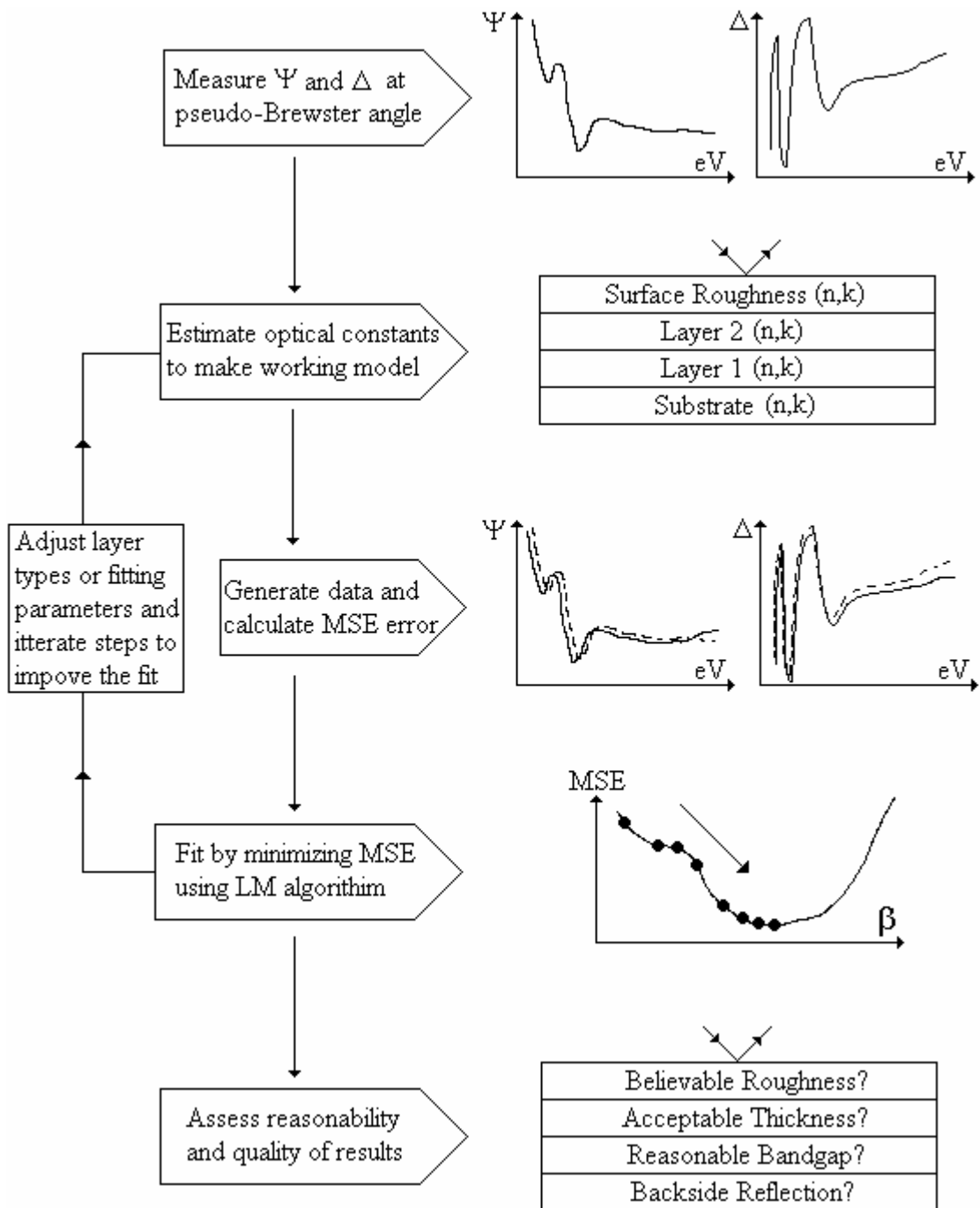


Figure 3.7: Flowchart of the standard iterative VASE data analysis procedure (after [24])

The first step after measurement is to obtain as much information about the sample as possible so that a reasonable optical model can be established as a starting point. When studying common films, an effective approach is to use the material database included with the modeling software to create an initial optical model of the sample. While, the optical properties of these built-in layers can be deposition dependent, they are often a good place to start. Also, if samples with similar optical properties have previously been characterized then this data can sometimes be used as an initial model.

It is also important to have an idea about the film interfaces and surface texture. Ellipsometry data is a result of these boundaries and so information regarding the roughness as well as the change in optical constants across an interface is useful when constructing a model. Although it is difficult to model slow gradient changes between two films, jagged yet abrupt interfaces formed by crystalline materials can be modeled with a special technique. The optical effect of this extended transition region can be modeled by considering the jagged region itself to be a layer. This approach is known as the Bruggemann effective medium approximation (EMA) [25] and calculates the dielectric constant $\langle \epsilon_r \rangle$ of this pseudo layer as a weighted average of the constituent materials. In general, the EMA layer can be composed of two or more materials and the effective dielectric response is given by solving the following equation

$$f_1 \frac{\epsilon_{r1} - \langle \epsilon_r \rangle}{\epsilon_{r1} + 2\langle \epsilon_r \rangle} + f_2 \frac{\epsilon_{r2} - \langle \epsilon_r \rangle}{\epsilon_{r2} + 2\langle \epsilon_r \rangle} + f_3 \frac{\epsilon_{r3} - \langle \epsilon_r \rangle}{\epsilon_{r3} + 2\langle \epsilon_r \rangle} \dots = 0 \quad (3.13)$$

where the coefficients f_i are the fractional composition of each constitute. Typically the EMA layer is used to account for surface roughness by combining the optical constants of the top layer and void (air) with $f_1 = f_2 = 0.5$. The thickness obtained for this layer is primarily for fitting purposes and will only be in general agreement with the actual RMS roughness as measured by AFM.

After the initial optical model layers and interfaces are set, $\Psi(\lambda, \theta)$ and $\Delta(\lambda, \theta)$ are generated and compared with the measured data. To assess the agreement of fit between generated and experimental data a merit function is used, the most common being the mean-squared error (MSE)

$$MSE = \sqrt{\frac{1}{2N - M} \sum_{i=1}^N \left[\left(\frac{\Psi_i^{\text{mod}} - \Psi_i^{\text{exp}}}{\sigma_{\Psi_i}^{\text{exp}}} \right)^2 + \left(\frac{\Delta_i^{\text{mod}} - \Delta_i^{\text{exp}}}{\sigma_{\Delta_i}^{\text{exp}}} \right)^2 \right]} \quad (3.14)$$

where σ_i^{exp} is the standard deviation of uncertainty for the i^{th} data point (calculated from the spread of data recorded by the rotating analyzer), Ψ_i^{exp} and Δ_i^{exp} are the experimental data points obtained, Ψ_i^{mod} and Δ_i^{mod} are the model calculated points, N is the total number of data points, and M is the number of parameters in the model being fit. The use of σ_i^{exp} provides three advantages [26]: 1) parts of the spectrum that can be measured with greater accuracy are weighted more heavily, 2) if a different representation of the experimental data is chosen, $\rho_i^{\text{exp}} = \tan(\Psi_i^{\text{exp}}) \exp(i\Delta_i^{\text{exp}})$ for example, and uncertainty is propagated, the MSE will be equivalent, and 3) if the fit appears to be good, the MSE value can be used to gauge how reasonable the experimental uncertainty estimates are. If

the MSE is frequently much less than one for good fits, then the error bars may be too large and likewise $\text{MSE} \gg 1$ implies the underestimated error bars.

After establishing a merit function, an efficient method of reducing the MSE is needed. By expressing the model-generated parameters from eq. (3.14), Ψ_i^{mod} and Δ_i^{mod} , conceptually as $f(x_1, x_2, \dots, x_m; \beta_1, \beta_2, \dots, \beta_k)$ where $x_1, x_2, \dots, x_m = \bar{x}$ are the known or assumed parameters of the model, $\beta_1, \beta_2, \dots, \beta_k = \bar{\beta}$ are the parameters to be varied and f is the MSE merit function. It can be seen that reductions in MSE will be obtained by correctly adjusting the $\bar{\beta}$ values to travel down the MSE error surface. Typically this process is based upon one of two approaches; by iterating a Taylor series expansion under the assumption of local linearity, also known as Newton's method

$$f' = f(\bar{x}, \bar{\beta}') = f(\bar{x}, \bar{\beta}) + \sum_{j=1}^k \left(\frac{\partial f}{\partial \beta_j} \right) \delta \quad (3.15)$$

or alternatively by following the path of steepest decent using a gradient approach.

$$f' = f(\bar{x}, \bar{\beta}') = f(\bar{x}, \beta_j + A_j \delta), \quad A_j = \begin{cases} 1 & \text{if } f(\beta_j + \delta) < f(\beta_j) \\ -1 & \text{if } f(\beta_j + \delta) > f(\beta_j) \\ 0 & \text{if } f(\beta_j \pm \delta) > f(\beta_j) \end{cases} \quad (3.16)$$

These techniques approach the MSE minimum differently, both having drawbacks depending upon the curvature of the error surface as illustrated in Figure 3.8.

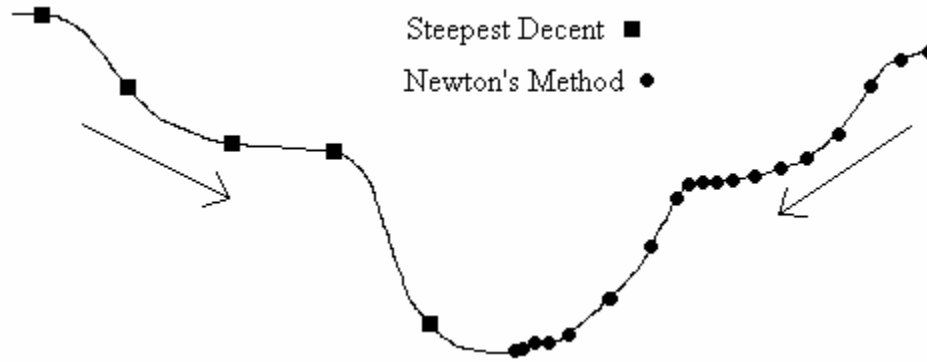


Figure 3.8: Simplified single parameter MSE fitting using Newton’s method and path of steepest decent.

The method of steepest decent fails to converge to the exact minimum and Newton’s method is often painfully slow when the surface is close to flat. Fortunately however, the advantages of the two approaches are complementary and an effective hybrid technique known as Levenberg-Marquardt (LM) algorithm [27] exploits this fact. Essentially, f' is chosen based upon a weighted average of the two approaches. When the MSE is large, the fit predominantly follows the steepest decent and when MSE is small or unchanging Newton’s method is favored. Additionally, the δ parameter shown in eqs (3.15) and (3.16) can be adjusted dynamically as the fit progresses.

Unfortunately, neither component of this hybrid approach is immune to settling in on local minima. It is best to “sample” the MSE surface by varying all the $\bar{\beta}$ parameters over a wide range of feasibility and checking the MSE at each permutation. The point with the lowest MSE is likely in the vicinity of the true minimum and the LM method can then be applied.

Technically, the final MSE value is dependent only upon the error bar estimation and effectiveness of the minimization algorithm. In practice, however, the MSE will also vary depending upon the type of sample being measured. Samples with complicated models will often result in significantly higher MSE values than simpler samples with fewer layers. Thus, considering the MSE in a subjective sense by comparing it to other samples fit with the same model is the best way to assess the relative quality of fit.

For well-characterized samples, this fitting technique is an accurate method of measuring layer thickness, fine-tuning optical constants, and resolving features such as crystallinity, anisotropy, and fractional composition. Often, however, no previous optical data is available for one or more layers in a sample. To find the optical constants of these materials, a dynamic layer is used which adjusts n and k of the unknown material until Ψ and Δ generated from the model are in agreement with the measured data. If the sample is formed by depositing a single layer at a time then a model can be built up by obtaining the optical constants and thickness of the topmost layer after each new layer is added. If possible, this approach is best because the optical and physical parameters of the sub-layers can be held fixed as the optical constants are fit for the surface layer. However, consideration of surface growth must be made to ensure that interface layers aren't introduced while the measurements are being performed.

The main difficulty in measuring optical constants of an unknown layer is the relationship between the variable parameters. The three significant adjustable optical parameters, n , k , and thickness, are often correlated and cannot be independently determined from only two measured quantities. For example Ψ , a measure of the

attenuation of the light, can be affected by either the thickness or the absorption (related to the optical constant k) of a layer. To overcome this constraint, the spectrum over which data is fit can be reduced to a region where the sample is transparent. In this region where the absorption, and thus k , is essentially zero, Δ undergoes sharp flips.

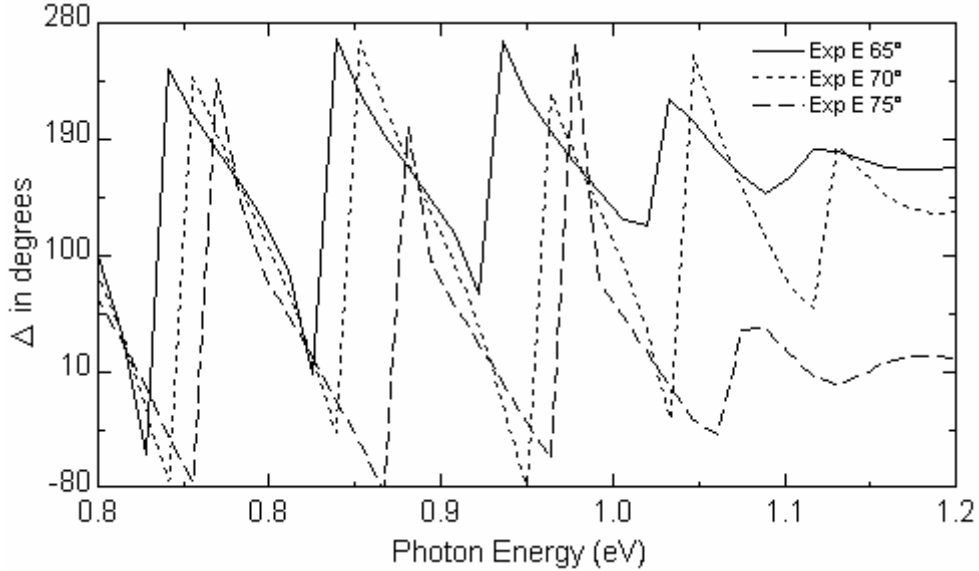


Figure 3.9: Sharp Δ flips of a $\text{Cu}(\text{Ga},\text{In})\text{Se}_2$ sample with a bandgap of approximately 1.1 eV (33843.21). The three lines correspond to incident angles of 65° , 70° , and 75° which span the pseudo-Brewster angle.

These flips are somewhat analogous to the interference fringes that are observed when a material of varying thickness is probed with a monochromatic beam of light. As shown in Figure 3.3, the index of refraction continues to change far off resonance where the absorption is essentially zero. To model this dispersion, a simple Cauchy function can be used.

$$n(\lambda) = n_0 + \frac{n_1}{\lambda^2} + \frac{n_2}{\lambda^4} \quad (3.17)$$

Although the Cauchy function is basically a curve fitting approach, it is very useful when determining the thickness of a sample in its transparent region.

After the thickness is set, the optical constants need to be determined over the full measured range. To do this a procedure known as a point-by-point fit [20] is applied. This approach applies the LM algorithm for each $(\Psi, \Delta, \lambda, \theta)$ data point (using the previous values of n and k as a seed value) to find a value for n and k that best reproduced this measured data. The point-by-point fit allows an initial estimation for optical constants over the full measured spectrum. The fit is usually extremely good but there are three flaws to this approach that usually prevent the accurate determination of optical constants. The first is that the thickness used for the point-by-point fit was established under the assumption of zero absorption. The small amount of absorption that is actually present in the sample may be significant enough to produce inaccuracies in the thickness. This error then propagates to the generated optical constants but can be minimized through successive iterations, see Figure 3.7. The second shortcoming is that because each point is calculated individually, any noise in the measured data gets mapped directly to n and k . This effect can be reduced slightly by smoothing the optical data. The third and most significant problem with the point-by-point fit is that each data point is calculated without regard to the rest of the spectrum leading to optical data that isn't physical. Returning to the Lorentz oscillator model, eq. (3.4), the index, n , is dependent

on the damping or absorption, represented by k . This dependence is expressed in Kramers-Kronig relations

$$\begin{aligned} n(E) - 1 &= \frac{2}{\pi} P \int_0^{\infty} \frac{E' k(E')}{E'^2 - E^2} dE' \\ \varepsilon_1(E) - 1 &= \frac{2}{\pi} P \int_0^{\infty} \frac{E' \varepsilon_2(E')}{E'^2 - E^2} dE' \end{aligned} \tag{3.18}$$

with P implying that only the principle of the integral is taken. By knowing either the real or imaginary part of N or ε , the complimentary component can be calculated using these relations. This approach is used in reflectometry where absorption is measured and then the index of refraction is found using eq. (3.18). This reflectometry approach suffers from series approximation errors and generally the ellipsometry method, calculating the real and imaginary parts independently, is more robust.

To address the problem of physicality, the tabulated optical constants generated from the point-by-point fit are reproduced using a summation of linear oscillators.

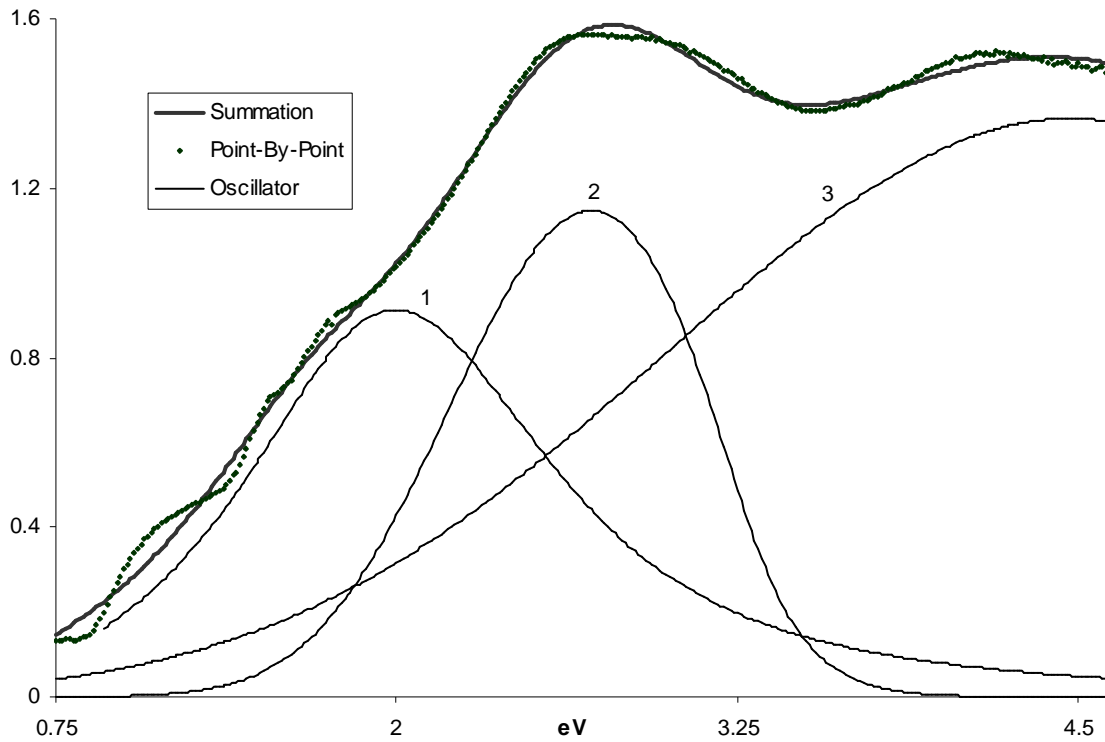


Figure 3.10: Point-By-Point generated data for k of a MoSe_2 sample which is reproduced by linearly summing three lorentz oscillators which are consistent with the Kramers-Kronig relations of eq. (3.18). Notice the unphysical low-energy ripples in the point-by-point data are removed using the oscillator model.

Using this general oscillator layer, the optical response of a material can be modeled in a physically correct manner using the point-by-point data as a guide. This step usually increases the MSE significantly but removes unphysical characteristics from the optical data. The parameters of each oscillator (FWHM, amplitude, energy) can be adjusted to lower the MSE.

After a general oscillator layer is established, the full optical model is in place and small improvements are made through iteration (see Figure 3.7). The thickness can be

adjusted slightly with a fit. Using this new thickness, a new point-by-point fit can be performed and the oscillators can be further corrected.

After successive iterations, the MSE will be maximally reduced. The final fitting step is to make adjustments to minor fitting parameters such as thickness non-uniformity, and backside reflections. These “non-ideality” factors will slightly reduce the MSE further and generally improve the appearance of the fit. When a final fit is achieved, with a low MSE and Kramers-Kronig consistency, the reasonability of the model must be considered. Although there are no fixed rules for this evaluation, there are three [18] prominent aspects of the model that should be judged.

First, are the resultant layer thicknesses within their expected range? If thickness results shrink to zero while fitting it is often because the optical constants of that layer are inaccurate. While this typically leads to poor fits, it can go unnoticed if the layer isn't optically significant (under a thick absorbing layer) or if the optical constants of another layer adjust to compensate for these inaccuracies. Second, is the surface roughness too large? The EMA model used for surface roughness is only accurate under 10nm. If the resultant thickness exceeds this then the surface roughness should be fixed at a reasonable value while parameters of other layers are adjusted. Third, do the optical constants of fit layers look believable? Semiconductors should exhibit “normal dispersion” below the bandgap (the index should increase with energy) and sharp oscillatory features should be scrutinized. For example, if a layer's modeled thickness is slightly off, this error will propagate dramatically into the calculated interference pattern. In order to compensate for the inconsistency between thickness and measured data, the

optical constants get distorted so that a good fit is maintained. Thus when iterating between point-by-point data and adjustments to a general oscillator layer, it can be helpful to vary the thickness slightly and note the effects.

If consistent and reasonable results with a low MSE are reached then it is quite likely that the optical model is correct but it should be understood that the uncertainty of ellipsometry results typically exceed the listed precision of the measurements.

Systematic errors such as monochromator and goniometer offsets, alignment drift as well as model deficiencies such as correlation or incorrect assumptions tend to outweigh acquisition noise. This is evident whenever collections of experimental values over a limited spectral range all lay slightly above or below the generated data as this cannot statistically be attributed to noise.

Chapter 4

EXPERIMENTAL

The base layers of the samples investigated in this work were provided by IEC using standardized deposition techniques [28]. Physical details of these layers (Figure 4.1) relevant to optical characterization will be mentioned briefly and information regarding sample preparation performed for this work will be described in more detail. Standardized measurement procedures are provided and alternative analysis techniques used to guide the optical modeling parameters or substantiate VASE results will be mentioned.

4.1 Deposition

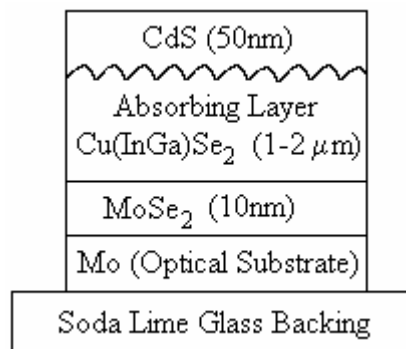


Figure 4.1: Schematic diagram of a typical Cu(In,Ga)Se₂ sample as prepared by IEC.

A 1x1 inch piece of Soda-Lime glass forms the substrate upon which the thin films are deposited. The glass pieces are first coated with approximately 0.8 μm of molybdenum through a sputtering process. The molybdenum layer reflects ~50% of incident light and is an order of magnitude thicker than its skin depth (at $\lambda \approx 1700$ nm) thus serving as the optical substrate. The texture of this layer closely follows the morphology of the glass substrate. RMS roughness measurements of the Mo films performed by atomic force microscopy (AFM) analysis yielded a value of <5 nm ensuring that the substrate is optically smooth.

The absorbing layer of the sample is the quaternary chalcopyrite $\text{Cu}(\text{In,Ga})\text{Se}_2$. 1.5-2 μm of this polycrystalline material is deposited on the Mo substrate using a four source co-evaporative system. Details regarding deposition rates and conditions can be found elsewhere [29]. These standard deposition conditions yield a thin ($\sim 100\text{\AA}$) layer of MoSe_2 between the Mo and $\text{Cu}(\text{In,Ga})\text{Se}_2$ layers [30] which assists the electrical contact across the interface. The bandgap of $\text{Cu}(\text{In,Ga})\text{Se}_2$ is a function of Ga incorporation and ranges from 1.04 to 1.68 eV [13] for CuInSe_2 and CuGaSe_2 respectively. The samples prepared in the work had Ga/(In+Ga) ratios of approximately 0.3 which corresponds to a bandgap of $\sim 1.2\text{eV}$. Cu (% at) composition was kept between 23-25% [31]. The grains of this film have diameters on the order of 1 μm and thus the surface is significantly rougher than the Mo or glass subsurface. AFM measurements on this surface yielded MSE roughness values of 50-100 nm

The final deposited layer for samples analyzed in this work is cadmium sulphide (CdS). This layer was formed through a solution growth or chemical bath deposition (CBD) process where Cu(In,Ga)Se₂ samples are immersed in a heated bath of reacting chemicals. The growth rate can be controlled by adjusting the pH, temperature, and relative concentrations of the reactants incorporated in the bath [17]. The specific recipe used for this work involved adding 22mL of 0.015M CdSO₄, 22mL of 0.14M SC(NH₂)₂, and 28mL of 1M NH₃ to 150mL Nanopure H₂O. The solution beaker is immersed in a water bath fixed at 65° C with a magnetic stirrer used for agitation. During the first minute, only the CdSO₄ and NH₃ are added to the H₂O. This combination serves as an ammonia etch to clean the Cu(In,Ga)Se₂ surface [32]. After 1 minute, the SC(NH₂)₂ is added and the heterogeneous ion-by-ion growth of CdS on the substrate surface begins. In order to prevent CdS particles that form homogeneously in the solution from depositing onto the surface, the CBD is limited to 12 minutes. To form a thicker CdS layer, the CDB recipe can be repeated.

This CdS layer has a higher bandgap around 2.5eV and thus serves as a junction forming window layer. Its surface follows the morphology of the Cu(In,Ga)Se₂ layer beneath it and unfortunately falls short of the “optically smooth” criterion of ellipsometry.

4.2 Sample Preparation

In order to obtain reflection data of sufficient intensity from a Cu(In,Ga)Se₂ sample, a specular and clean surface must be obtained. The most straightforward

approach is to etch or polish the rough surface. This method used by Alonso [11] involves a hydrofluoric acid etch, followed by multiple slurrie and chemomechanical polishings to ensure that the surface composition is not modified. For this work a simpler two-step etch procedure was used. First an aqueous bromine solution [33] is used to smooth the surface. 16-17 drops of Br_2 is added to 100 mL mixture of dionized H_2O and 4.0 g KBr powder (used to improve the solvency of the Br_2). This etch was carried out at room temperature with gentle agitation. The effectiveness of this etch decreased with both time (Br evaporation) and sample etching and so the solution was always freshly prepared and never reused for successive etchings.

Immediately following the Br etch, an aqueous KCN solution [34] was used to etch clean the surface of remnant Se [35]. The concentration of this etch was 0.1M and the pH was set to 12 to prevent the formation of lethal HCN gas. This etch was performed at 70° C for 1 minute with gentle agitation. The samples were rinsed in dionized water and then dried under nitrogen or argon gas.

An alternative method, of obtaining a smooth polycrystalline $\text{Cu}(\text{In,Ga})\text{Se}_2$ surface was developed by developed by P. D. Paulson [13]. Measurements are performed on the reverse side of the $\text{Cu}(\text{In,Ga})\text{Se}_2$ film after it is peeled from the Mo optical substrate as shown in Figure 4.2.

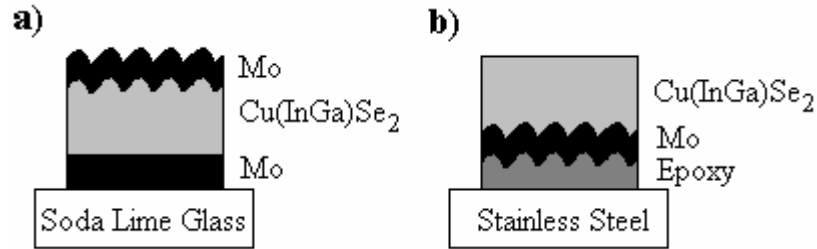


Figure 4.2: Cu(In,Ga)Se₂ sample preparation before (a) and after (b) using peeling method (after P. D. Paulson [13]).

This sample is formed by first sputtering a second layer of the well characterized Mo onto the rough Cu(In,Ga)Se₂ surface. Next steel backing is glued with standard office epoxy to this Mo layer. Allowing a day to dry, the steel backing is placed in a vice and peeling pressure is applied to the other backing (glass). The separation occurs cleanly at the interface of weakest adhesion, the Cu(In,Ga)Se₂/MoSe₂ interface. The peeled Cu(In,Ga)Se₂ surface has a RMS roughness of 5-10 nm and thus can be analyzed using ellipsometry. One difficulty encountered with this procedure involved the slight curving of the steel backing after a peel. Because samples are suctioned to a vertical stage, bends in the substrate can lead to slight alignment drifts while data is being taken. For this reason, alignment was always re-checked on peeled samples after measurements had been made. If excessive drifting occurred then the sample data was discarded.

CBD films of CdS were prepared on two different substrates for VASE analysis. Initially, CdS was deposited upon Mo/Soda-Lime glass substrates because the Mo optical substrate was well characterized and allowed a simpler optical model. CdS films were also deposited upon both peeled and etched layers of Cu(In,Ga)Se₂. A collection of

samples were annealed to check for changes in optical properties and crystallinity. The annealing was performed in a glass tube flushed with argon gas.

4.3 VASE Measurement

The most effective method of building an optical model for ellipsometry analysis is to collect optical data by adding a single layer at a time. The optical response of each layer is different and thus the VASE measurement settings differ slightly. In all cases however, measurements were made across the full spectral range (0.75-4.6eV) at room temperature immediately following the sample preparation steps. Unless otherwise noted, samples were measured as “isotropic + depolarizing” with a dynamic maximum of 100 revolutions per measurement.

Due to its high index value, the Mo substrate was measured at 70°, 75°, and 80°. Ψ and Δ varied slowly and smoothly so data was taken with a relatively large step size of 0.025eV. AFM measurements were performed to independently establish a surface roughness for modeling purposes. MoSe₂ data was obtained from both selenized Mo samples (grown at $T_{\text{substrate}}=400^{\circ}\text{C}$ for 90 minutes) and on the glass backing side of peeled Cu(In,Ga)Se₂ samples. Data was taken at 65°, 70° and 75°, with a step size of 0.0125 eV.

Cu(In,Ga)Se₂ samples prepared by either peeling or etching techniques were measured under a steady flow of nitrogen gas to prevent surface contamination. Data was acquired at three angles of incidence; the pseudo Brewster angle, 70° and $\pm 5^{\circ}$. The energy step size was varied throughout the measurement. In the lowest energy region, 0.75-1eV, where Δ fluctuates rapidly, data were recorded every 0.01 eV. In the bandgap

region, from 1-1.6eV, Ψ and Δ were recorded in steps of 0.005 eV to accurately resolve the absorption edge. Finally, in the range of 1.6-4.6 eV, Ψ and Δ fluctuate much more gradually and data was recorded with a step size of 0.025 eV. Unfortunately, version 3.337b of the VASE32 software doesn't allow these measurements to be scheduled one after another so care was taken to set the next range and step size immediately following the completion of the previous run. After the data was collected, the experimental files were merged and data continuity at 1 and 1.6eV was verified by inspection. All Ψ and Δ measurements were performed with dynamic averaging of at least 200 revolutions per measurement to reduce noise which is more prevalent in the high energy region.

Samples prepared by either peeling or etching produced similar Cu(In,Ga)Se₂ surfaces but with differing optical sublayers. These differences were represented in the corresponding optical models shown in Figure 4.3.

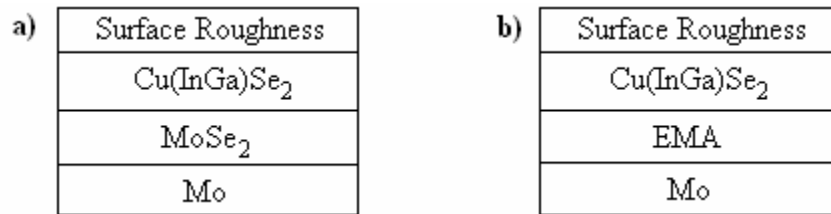


Figure 4.3: Optical models used to model samples prepared by etching (a) or peeling (b) methods.

CdS samples showed no optical changes after being exposed to air and so VASE data was taken without nitrogen gas flow. Incident angles were 65°, 70°, and 75° with a step size of 0.0125eV.

4.4 Non-VASE Analysis

Four additional analysis techniques were used in this work to independently confirm VASE results or to provide guidance when creating an initial optical model.

A Digital Instruments Dimension 3100 AFM was used at the primary measurement technique of film surface roughness. $5\mu\text{m} \times 5\mu\text{m}$ surface scans were recorded with integral and proportional gains of 0.3 and 0.6 respectively. From this scan, a relatively smooth $\sim 2\mu\text{m} \times \sim 2\mu\text{m}$ region was selected and statistics such as RMS roughness and Z-range from this region were considered when establishing etch rates and optical models.

An enclosed AT261 DeltaRange scale with $\pm 0.05\text{mg}$ accuracy was used to determine mass loss and thus etch rate of bromine etchings. For each measurement, the sample was first blown clean with a nitrogen gas gun and the scale was re-zeroed. Three measurements were taken and the average was recorded.

The optical properties of $\text{Cu}(\text{In,Ga})\text{Se}_2$ films change as a function of relative Cu or Ga incorporation, and thus the elemental composition needed to be established to properly model this layer's optical constants. This was done using an Oxford 6900 Energy Dispersive Spectroscopy (EDS). Data was taken with a working distance of 31mm, a magnification of 1000X, 20kV beam, and a condenser lens setting that produced a detector dead time of 35-40%

The crystal structure of thin CdS films were analyzed using Glancing Incident Angle X-ray Diffraction (GIXRD) from a Rigaku D/Max 2200 instrument. To collect

data on a single 50nm film, the incident angle was set to its minimum or critical angle of 0.3° . Asymmetric detector measurements were recorded from 20° - 50° with a step of 0.05° .

Chapter 5

RESULTS

The optical properties of various films as prepared in high performance Cu(In,Ga)Se₂ cells were measured using a VASE. This data is presented in terms of the optical constants rather than the dielectric constants because the former is more typically encountered when studying the behavior of light in a PV cell. Additionally, the dielectric behavior more directly represents physical properties of the films such as band structure which isn't the focus of this work.

Non-destructive analysis techniques allowed each layer of a given sample to be systematically analyzed before additional layers were deposited. This procedure of obtaining unique optical data for all layers of each individual sample (rather than use optical constants for sublayers which were obtained from previous samples) was followed whenever possible and eliminated the error potentially induced by the slight variations between identically prepared samples.

5.1 Mo

The optical constants of a Mo were determined using a simple optical model consisting of an optically thick Mo substrate with a surface roughness layer. The initial

optical constants used for the Mo layer from Palik [5] were available in the WVASE 32™ software. This data was adjusted using a point-by-point fit until the model matched the measured Ψ and Δ data. Experimental Ψ and Δ data obtained from different samples across different runs showed little variation or change with time. This was taken as an indication that no significant oxidation layer formed on the Mo surfaces when exposed to air and no attempt was made add this oxide layer or account for the possibility of surface Na when modeling the Mo film.

Variations, shown in Figure 5.1 were observed in n and k as the modeled surface roughness was adjusted. The point-by-point and surface roughness fittings could not be performed simultaneously and so the modeling procedure required that a roughness value be chosen rather than fit. This modeled roughness is only a mathematical approximation however and can only be correlated with AFM measurements to within a factor of two. Additionally, MSE values could not be used to establish which roughness produced the best fit because the point-by-point fit simply compensated for whatever roughness was chosen.

To resolve this problem, Mo optical constants were generated for multiple roughness and then used as the substrate when modeling the thin MoSe₂ layer on peeled Cu(In,Ga)Se₂ samples. The Mo optical constants produced when modeled with a 20Å roughness consistently allowed the lowest MSE fits of the MoSe₂ layer. Therefore this set of optical constants is accepted as being the most accurate.

Differences in n and k were also observed between Mo films sputtered on Soda-Lime and 7059 glass backings. This difference is most likely due to Na diffusion which occurs in Soda-Lime samples [4].

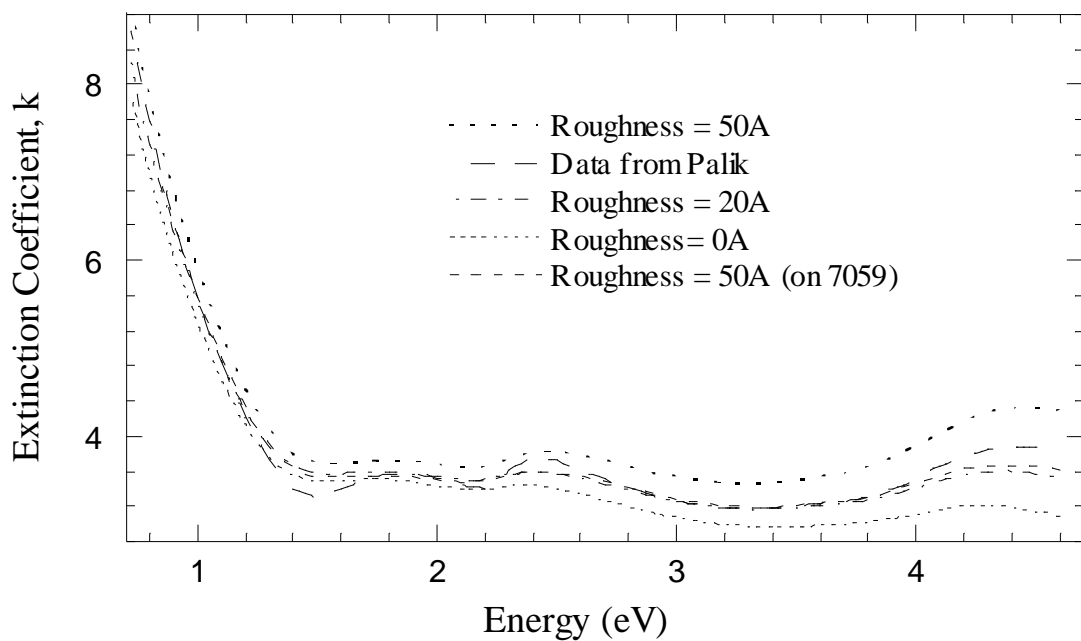
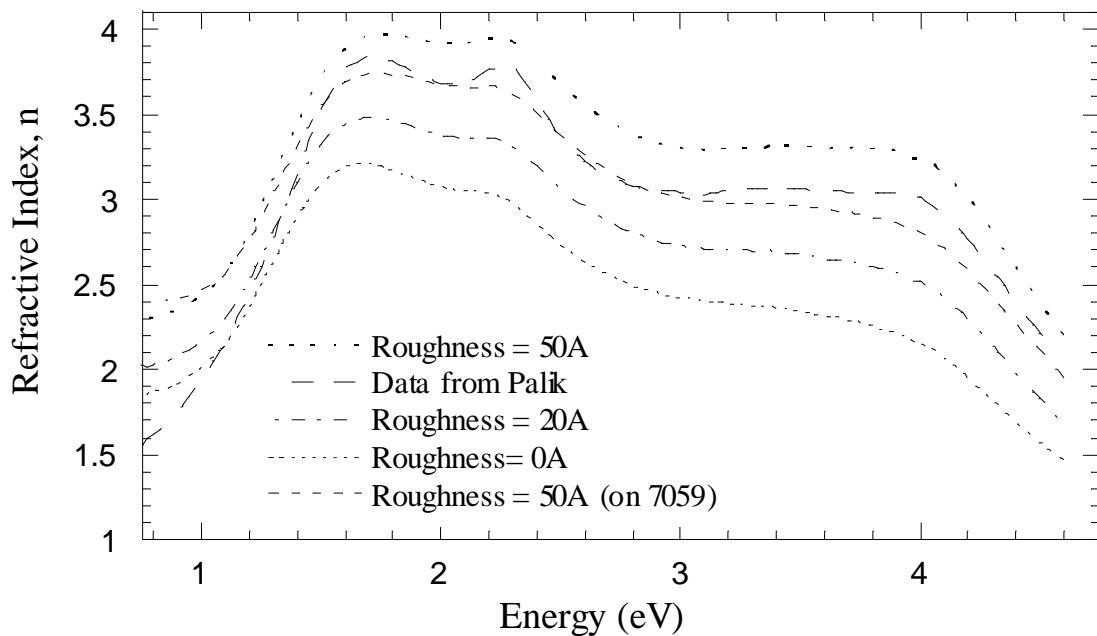


Figure 5.1: Mo optical constants obtained from VASE models. Variations in the modeled surface roughness significantly influence n . The effect of Na diffusion can be noted by comparing the optical constants of samples prepared on Soda-Lime with 7059 glass.

5.2 MoSe₂

Generally it is difficult to simultaneously measure the thickness and optical constants of very thin films ($<100\text{\AA}$) because the influence of the film on reflected intensity is minimal. Reported MoSe₂ thickness for high efficiency Cu(In,Ga)Se₂ cells are approximately 100\AA [30] and so characterization of this layer could not be approached directly. Instead a thicker layer of MoSe₂ ($\sim 500\text{\AA}$) was grown by exposing a heated Mo/Soda-Lime substrate to selenium gas ($T_{\text{substrate}}=400^\circ\text{C}$, Deposition Time=90 min - a process similar to [36]). With this approach, an accurate determination of thickness was obtained using a Cauchy layer (Eq. 3.17). Next a Kramers-Kronig consistent layer was formed by representing this Cauchy data with a summation of three general oscillators. The fitting process was iterated (Figure 3.7) until a final MSE of around 6.8 was obtained.

Ideally the final MSE is much closer to 1-2 but in this case the higher value is indicative of errors in both the MoSe₂ and Mo layers. Comparing the MoSe₂ point-by-point and general oscillator data shown in Figure 5.2 illustrates this error. If the Mo optical constants were exact and the MoSe₂ surface perfectly clean, then the point-by-point and general oscillator data would exactly coincide. The result, that inaccuracies in each layer tend to sum as more layers are added, emphasizes the need for accuracy as multiple layer samples are analyzed. Fortunately, in this case the point-by-point data fluctuates about the oscillator fit indicating that the errors are uncorrelated.

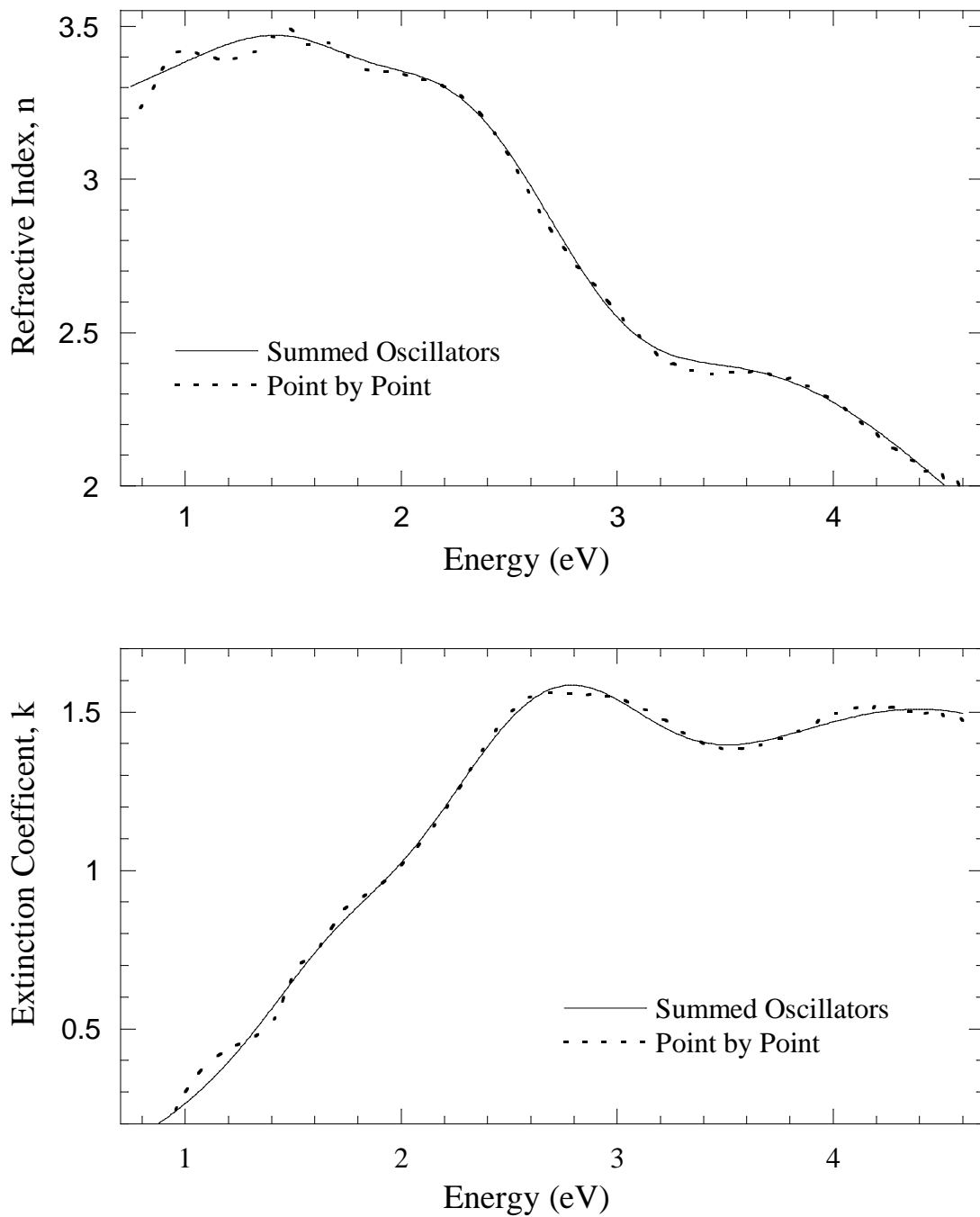


Figure 5.2: Differences between a general oscillator model and a point-by-point fit of a selenized MoSe_2 sample. These slight differences indicate that the Mo data in the optical model is slightly inaccurate and that this error could propagate to the MoSe_2 fit.

The optical constants measured for a selenized sample were then used as MoSe₂ data in the initial optical model for peeled samples. Previous work by Paulson [13] used XPS measurements to verify that the peeling procedure causes a clean separation at the MoSe₂/Cu(In,Ga)Se₂ interface. This was also confirmed optically by the failed attempt to fit peeled samples with a thin surface layer of the material on the opposing side. The exposed MoSe₂ film of peeled samples showed no observable change in measured Ψ and Δ values after exposure to air. The agreement of measured Ψ before and after exposure to air is shown in Figure 5.3. This agreement indicates that no optically significant oxide layer is formed on exposed MoSe₂ layers and thus a surface oxide layer was not used when modeling the peeled MoSe₂ samples.

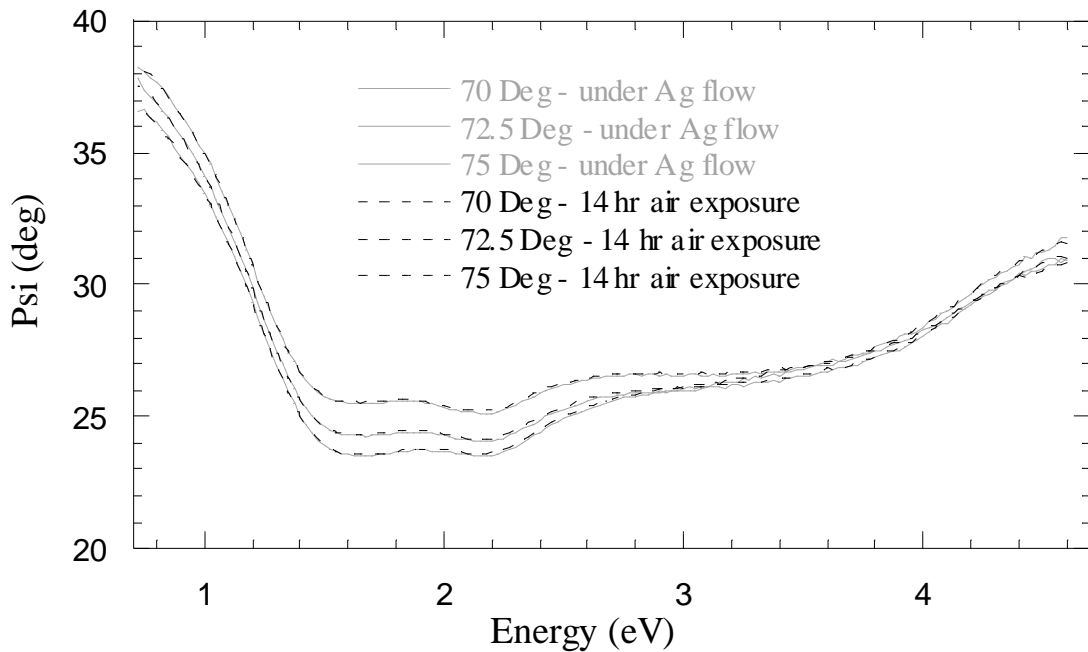


Figure 5.3: Ψ measured first under Ar flow immediately after peeling and then again after 14 hour exposure to air at room temperature.

The initial optical data from the selenized sample was used to establish the thickness of the MoSe₂ film. After fixing this thickness, a point-by-point fit produced approximate optical constants which were then refined with a general oscillator model. This data is shown in Figure 5.4 for two peeled MoSe₂ films of different thickness (sample numbers: 167Å=33844.13, 66Å=33843.13) and compared with data from the selenized sample.

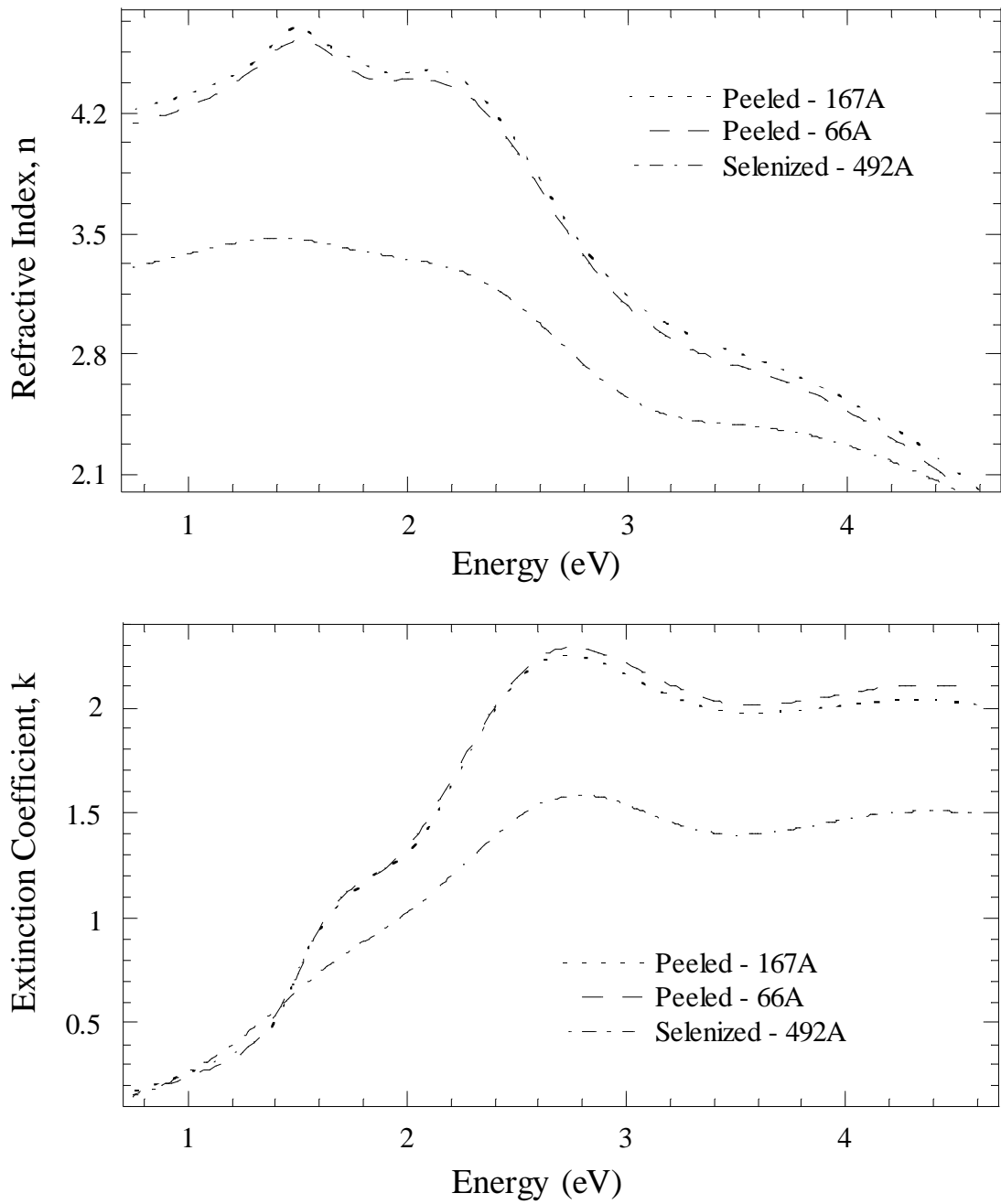


Figure 5.4: MoSe₂ optical constants obtained from VASE analysis on peeled and selenized samples. The close agreement for the two peeled samples suggests that the optical properties of the MoSe₂ layer in high efficiency devices are consistently different from films prepared by selenization.

5.3 Cu(In,Ga)Se₂

The primary technique used to prepare optically smooth Cu(In,Ga)Se₂ samples was through a chemical Br etch. Prior studies [33] on this technique suggest recipes over a broad range of Br concentrations (0.02-0.25M) and etch times. A standard recipe was required to optimally and consistently smooth samples analyzed for this work. To determine the Br₂/H₂O ratio that provided the smoothest etch, identical Cu(In,Ga)Se₂ samples were etched over a range of times and concentrations. Precise mass measurements made before and after etching were used to determine the change in thickness and thus the etch rate. Initial results indicated that over the range of Br concentrations tested (0.01-0.1M) the rate of etch was linearly proportional to the amount of Br₂ added. The desired reduction in Cu(In,Ga)Se₂ film thickness was established as the peak to valley z-range of the unetched film ($\approx 0.5\mu\text{m}$) as measured by the AFM. After narrowing the range of effective concentrations and etch times, a controlled series of etches shown in Figure 5.5 was used to establish the standard recipe.

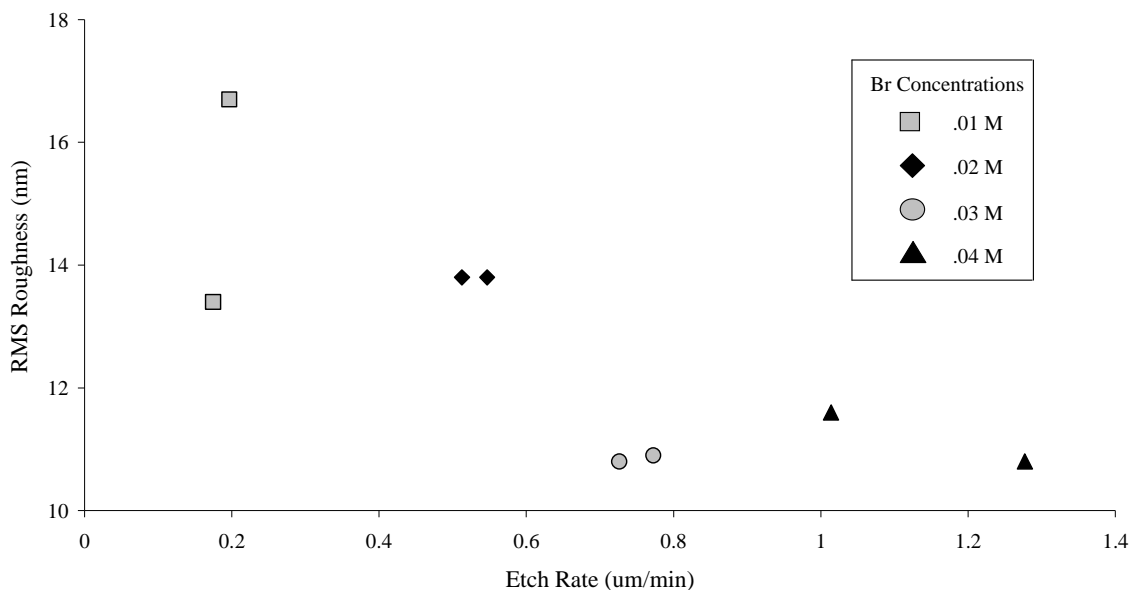


Figure 5.5: RMS roughness of Cu(In,Ga)Se₂ films etched under a range of Br₂ concentrations and times. For consistency, etch times (180, 220, 90, 110, 60, 75, 45, and 55 seconds as shown from left to right) were based upon the concentration so that all films underwent approximately equal changes in thickness ($0.6\mu\text{m} < \Delta_{\text{thickness}} < 0.9\mu\text{m}$). The change in film thickness for all samples shown was greater than the initial z-range roughness.

Based upon the results shown in Figure 5.5, a 60 second etch with a 0.03M Br concentration provided the smoothest surfaces without excessive loss of Cu(In,Ga)Se₂ film and was set as the standard recipe used for all etched samples prepared for this work. Although results by Canava [34] yielded a 2.5x smoother surface, the etched films in this work still met the primary requirement of being optically smooth. AFM measurements taken before and after etching are included in Figure 5.6.

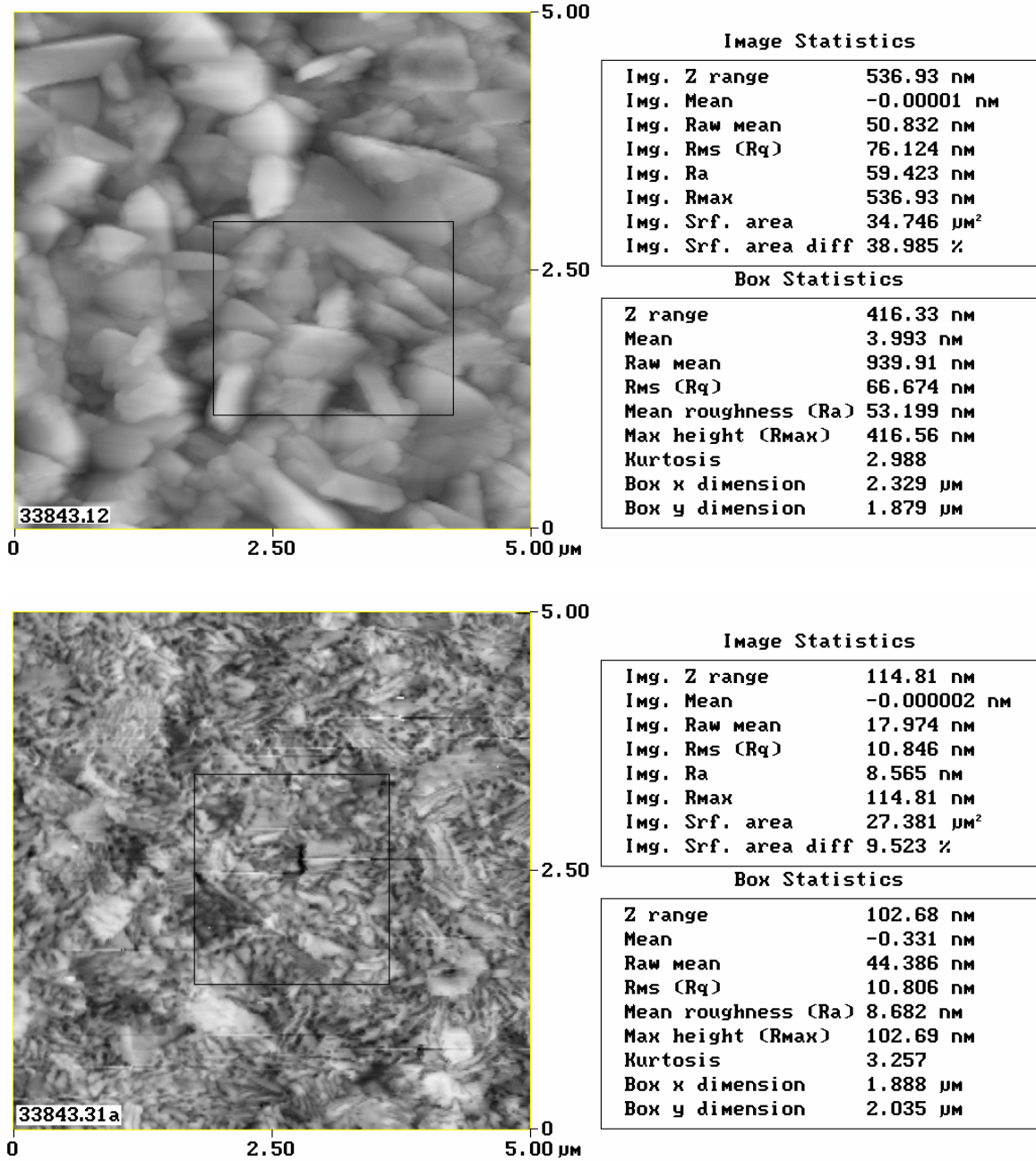


Figure 5.6: AFM images taken before and after applying a standard etch of 0.03 M Br₂ for 60 seconds. The etched RMS is approximately 10nm which satisfies the optically smooth criterion well beyond 4.6 eV.

While the Br etch is an effective means of smoothing the Cu(In,Ga)Se₂ surface, it unfortunately does not leave a clean surface. XPS measurements by Canava [34] determined that a remnant layer of Se is left on the surface and that this layer can be removed with a KCN treatment. This same etch was applied for a shorter period of time (60 seconds) to prepare samples for VASE analysis which is generally quite sensitive to surface layers. However, ellipsometry data taken before and after the KCN etch was nearly identical and when modeled, produced indistinguishable optical constants. This suggested that either a residual Se layer was not forming or that the KCN etch wasn't being applied for a long enough period to remove the layer. However, both guesses were refuted when samples were analyzed as devices. Three samples were prepared; one with only a Br etch, one with Br + KCN etches, and one with a Br etch and afterwards baked at 300°C under roughing pump vacuum to remove excess Se. The sample etched only with Br had poor device performance and I-V curve characteristics but both the KCN and baked samples recovered much of the efficiency and had a significantly higher I-V curve fill factor. This data is shown below in Table 5.1.

Table 5.1: Cell performance with different Cu(In,Ga)Se₂ etches and heat treatment. Samples marked with * indicate results shown are after a 2 minute heat-treat of the completed device at 200°C in air. Other samples did not improve with this treatment.

Sample	Treatment	Eff (%)	V _{oc} (Volts)	J _{sc} (mA/cm ²)	FF (%)
33888.22	As-deposited	15.8	0.623	33.2	76.3
33888.32 *	Br-etch	3.2	0.470	23.3	43.1
33888.33 *	Br-etch / KCN etch	11.2	0.524	29.8	72.1
33888.23	Br-etch / HT	12.8	0.575	30.1	73.9
33888.31	KCN-etch	12.7	0.537	32.7	72.7
33888.12 *	HT	13.6	0.569	32.1	74.2

This experiment suggests that the remnant Se layer exists after the Br etch but is not optically significant. For consistency however, all etched Cu(In,Ga)Se₂ samples were prepared with both Br and KCN treatments.

Unlike the thin MoSe₂ layer, the Cu(In,Ga)Se₂ layer is thick and has a fairly high absorption rate above the bandgap. The result is that little light gets transmitted to the Mo substrate and reflected back out to the detector. For this reason, the optical model is less sensitive to the Mo and MoSe₂ sublayers.

The optical model used for etched samples included a MoSe₂ sublayer with a thickness to be determined by the fitting algorithm. However, the MoSe₂ thicknesses established by this technique were inconsistent and often yielded a value of zero. To investigate this anomaly, a series of measurements were made on samples from a single Cu(In,Ga)Se₂ run that were thinned to different thickness using a range of etch times (0.03M Br). The optical constants of all layers were fixed and only the thicknesses of the

MoSe₂ and Cu(In,Ga)Se₂ layers were fit. For samples with a thinner Cu(In,Ga)Se₂ layer, the expectation was to see a strengthening of the MoSe₂ sensitivity represented by a more accurate fit of the layers thickness. The Mo/MoSe₂ side of a peeled sample was measured and the MoSe₂ thickness was found to be 168Å .

Table 5.2: MoSe₂ thickness for Cu(In,Ga)Se₂/MoSe₂/Mo samples with successively thinner Cu(In,Ga)Se₂ surface layers as fit by the VASE. Surface roughnesses were also fit except in the case of sample 33844.31b which was limited to a maximum value of 50Å to ensure physicality.

Sample #	MoSe ₂ Thickness	Cu(In,Ga)Se ₂ Thickness	Surface Roughness	VASE MSE
33844.23a	49Å	20580Å	36Å	14
33844.23b	0Å	18400Å	28Å	16
33844.31a	96Å	10070Å	29Å	75
33844.31b	198 Å	7430Å	~ 50 Å	38

With the exception of sample 33844.23b, the results in Table 5.2 indicate greater sensitivity to the 168Å thick MoSe₂ sublayer as the Cu(In,Ga)Se₂ film was thinned. However it should be noted that the quality of fit as determined by the MSE was relatively poor especially in the case of 33844.31a. Furthermore, the MSE values were not strongly dependent upon the value selected for the MoSe₂ thickness. For the samples shown above, adjusting the MoSe₂ thickness by a factor of two resulted in the MSE increasing by approximately one. This demonstrates what little sensitivity VASE has to layers beneath thick absorbing layers like Cu(In,Ga)Se₂.

Of all the layers analyzed in this work, Cu(In,Ga)Se_2 is the most complicated and difficult to model. Detailed studies relating the physical properties of this chalcopyrite structure with its optical behavior can be found elsewhere [9, 10, 11, 13, 37]. These studies primarily focus on the behavior of the bandgap which is triply degenerate due to crystal field splitting and spin-orbit interaction. This degeneracy is modeled optically using three parametric Gaussian broadened polynomial superposition oscillators [12] as shown in Figure 5.7 for an etched sample.

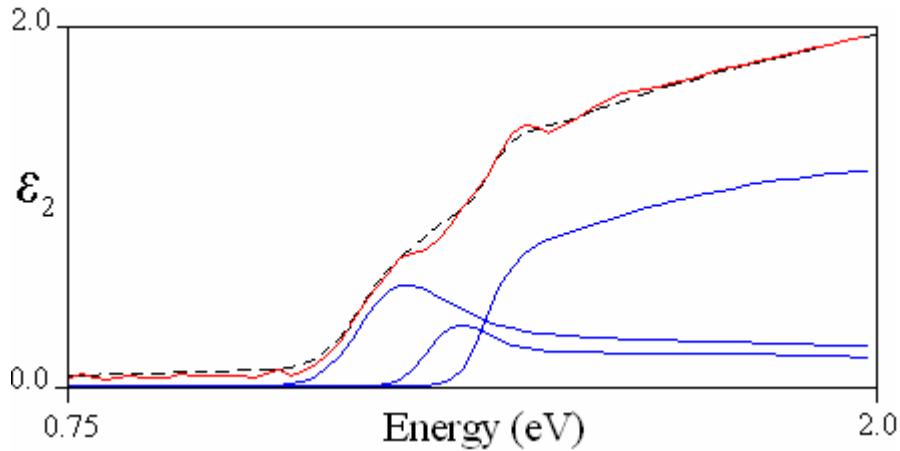


Figure 5.7: Three general oscillators used to model the bandgap of the Cu(In,Ga)Se_2 layer. The sharp onset of these transitions was described using asymmetric Gaussian broadened polynomial superposition oscillators. The linear superposition of the three oscillators is represented by the dashed line and the solid line is the dielectric function produced by the point-by-point fit.

While the optical model used for etched samples, Figure 4.3a, was very successful in reproducing the measured Ψ and Δ across the spectrum, inaccuracies were evident near the bandgap region. These inaccuracies, illustrated by the disagreement between the

summed oscillators and the point-by-point fit shown in Figure 5.7, ultimately resulted in a higher MSE value. Similar difficulties were reported by A.M. Hermann [12] which he attributes to surface roughness. The overall agreement between measured and generated values for Ψ as well as the discrepancy near the bandgap can be seen in Figure 5.8. Measured and generated Δ data are in nearly complete agreement and are not shown.

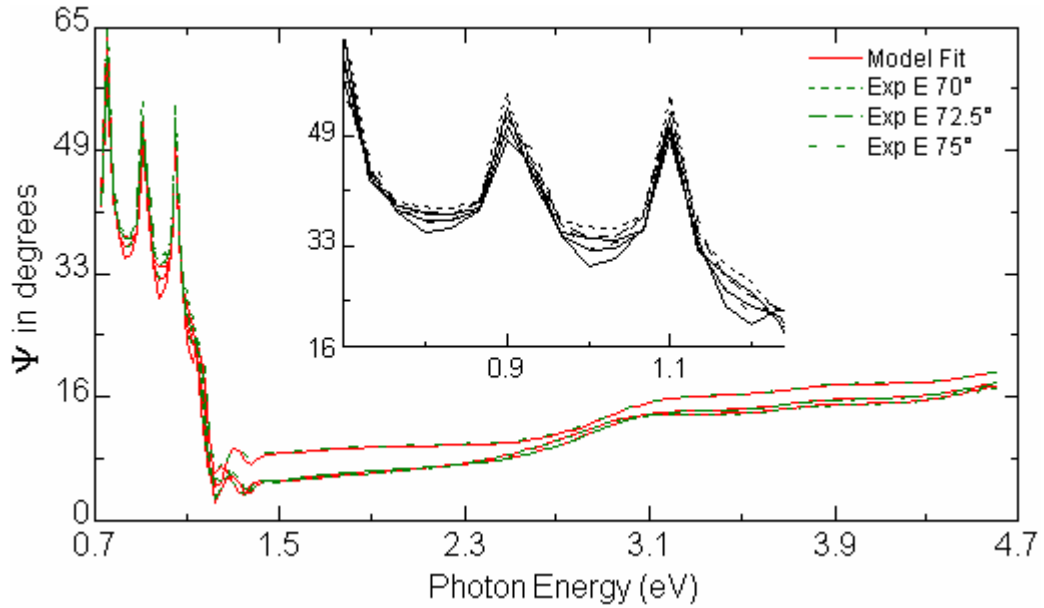


Figure 5.8: Measured and generated values of Ψ for an etched Cu(In,Ga)Se_2 sample. Dotted lines are measured data and the lighter solid lines are the data generated by the model. Disagreement between the model and data occurs around the bandgap region (1.0 -1.3 eV) shown more clearly in the inset image. A final MSE of 4.7 was obtained for this fit.

Typical MSE values for etched samples were around 4-5 while the MSE for peeled Cu(In,Ga)Se_2 was considerably smaller at around 0.5-2. Several attempts were made to compare the optical constants of peeled and etched samples by splitting a single

sample in two (to minimize the compositional variation that occurs in each run), etching one half and peeling the other. However the higher MSE of the etched samples prevented any precise differences from being observed consistently over the full measured range (.75-4.6 eV). As shown in Figures 5.9 and 5.10, the largest consistent differences between etched and peeled samples occur in the range 2.6-3.3 eV. In this region, both n and k of the etched samples are higher than the peeled samples. Unfortunately, a successful comparison between etched and peeled samples was only achieved for the two cases shown below and it remains unclear whether these differences were due to optical differences between the front and backside of the Cu(In,Ga)Se₂ films or were instead a result of the higher final MSE of the etched sample models. The optical constants of peeled samples measured for this work were in very good agreement with the results of Paulson and can be found elsewhere [13] in detail.

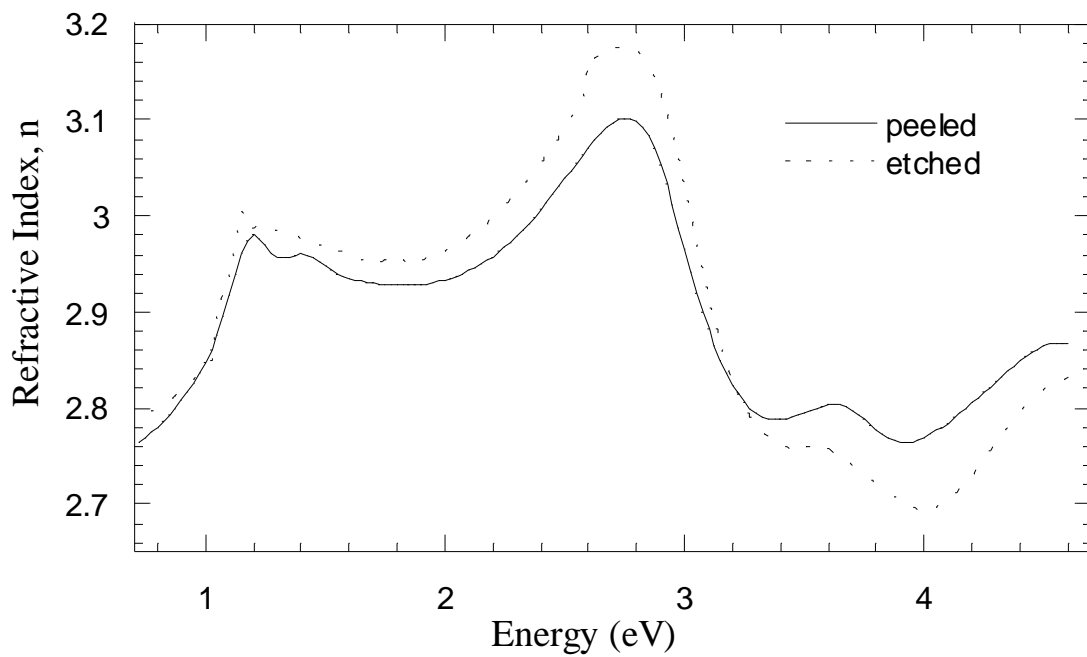
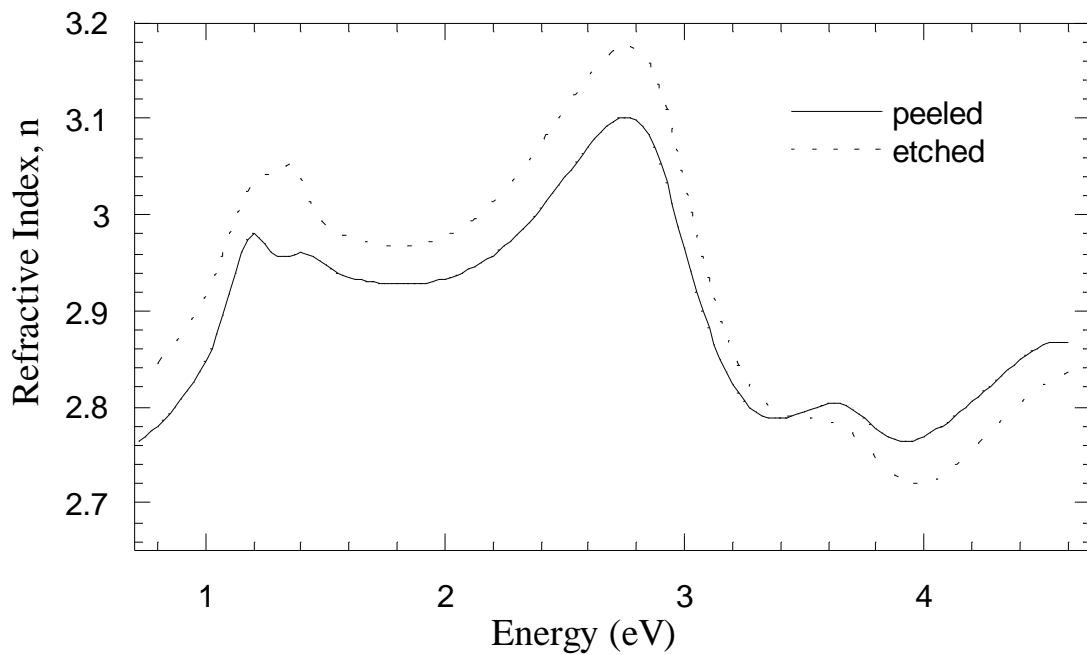


Figure 5.9: Differences in the refractive index n for peeled and etched samples. The samples were from runs 33843 (top) and 33845 (bottom).

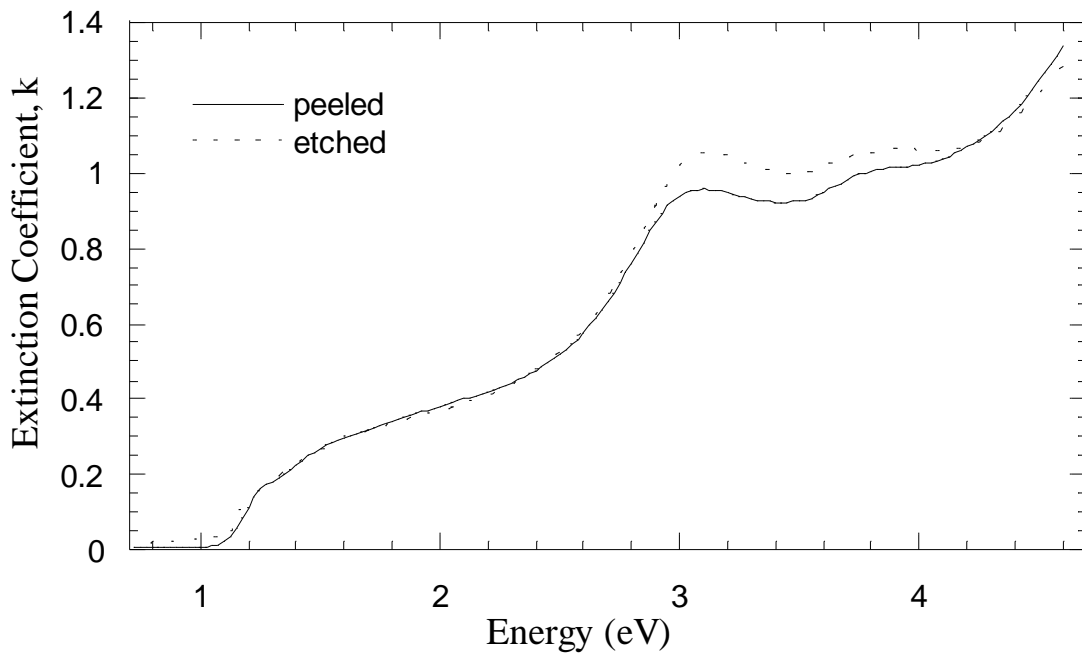
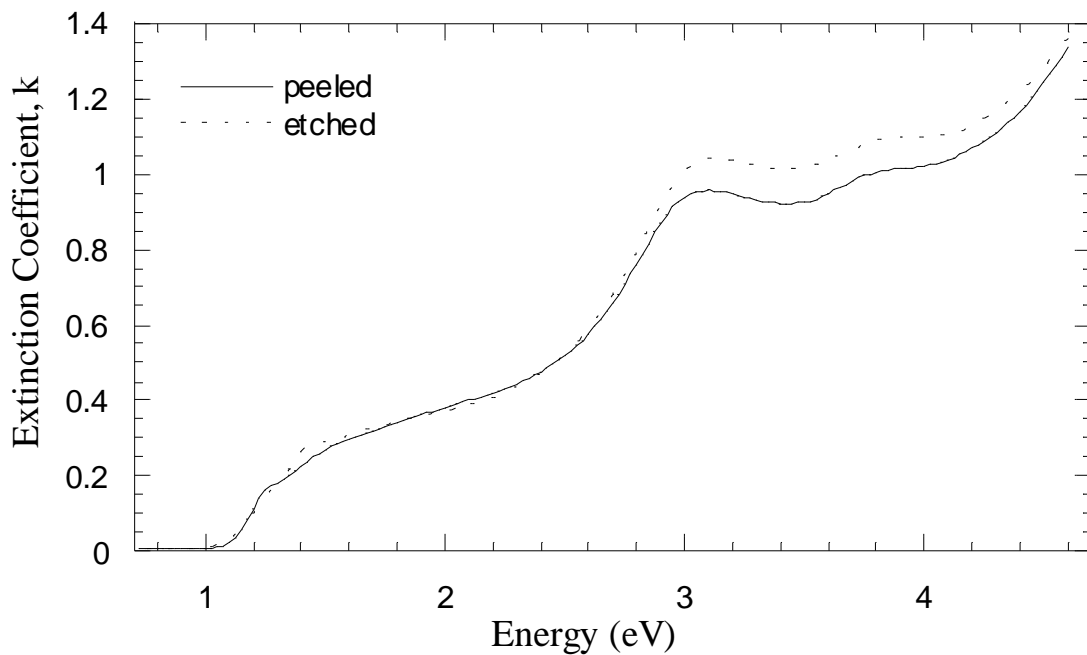


Figure 5.10: Differences in the extinction coefficient k for peeled and etched samples. The samples were from runs 33843 (top) and 33845 (bottom).

5.4 CdS

Initially the CBD CdS layer could not be analyzed on top of Cu(In,Ga)Se₂ because the optical constants of CdS were not well established for thin films or available in the VASE database [5]. Ψ and Δ are far more sensitive to the Cu(In,Ga)Se₂ layer due to its lower bandgap, higher absorption, and greater thickness. Any inaccuracies in the Cu(In,Ga)Se₂ model layer would be incorrectly compensated for by dramatically adjusting the optical constants of the CdS layer. For this reason, optical constants for CdS were first obtained in samples where a simpler optical model could be used; CdS deposited on a Mo/7059 substrate. Mo was chosen as the optical substrate because it had been previously characterized with the VASE and it was assumed that the CdS/Mo interaction would be minimal due to the relatively low CBD temperatures. A single bath deposition produced approximately a 50 nm film. This thickness could be effectively modeled using the Cauchy dispersion relation. Unfortunately, the optical constants obtained from fixing the thickness and applying a point-by-point fit contained significant low energy absorption between 0.75 and 1 eV. This type of absorption is typical with free electrons in metals ($\gamma = 0$ in equation 3.4) but was assumed to be unphysical in the case of CdS. When modeled with general oscillators, this low energy absorption was ignored and the point-by-point data from successive fitting iterations (Figure 3.7) did not reproduce this unphysical effect. The optical constants established with this fitting method were reproducible.

Additionally, CdS films were studied after thermal annealing. GIXRD measurements were used to determine crystal structure and changes in crystallinity.

Measurements were compared with JCPDS[®] (1997) standard cards. Results shown in Figure 5.11, establish a wurtzite phase with peaks at 28.15° (101), 26.85° (002), and 25.45° (100). The sharpening of these peaks confirms that crystallinity increases with annealing.

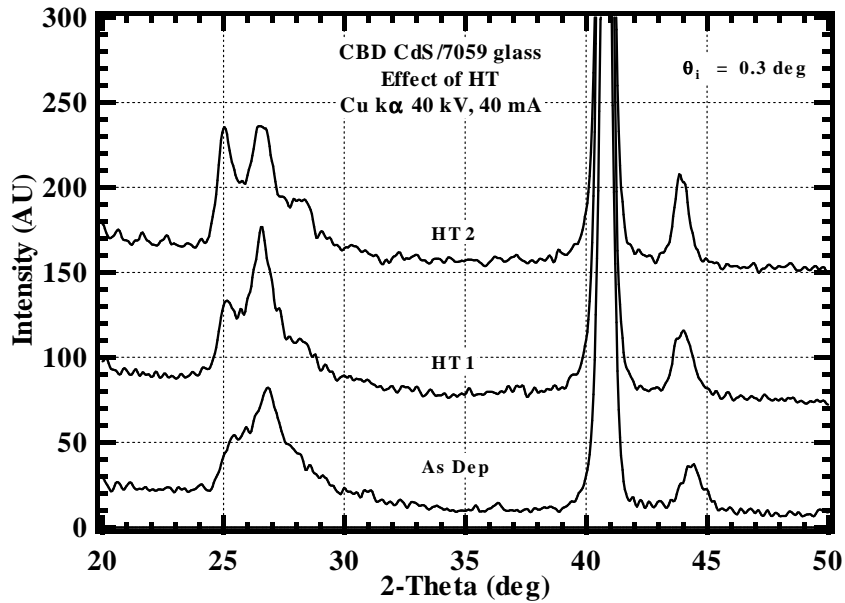


Figure 5.11: GIXRD spectra (offset for comparison) for a CdS/Mo/7059 sample after successive heat treatments of 20 minutes at 400° C (HT 1) and 30 minutes at 500 ° C (HT 2) in Argon. Data is shown using a three point binomial smooth and $\lambda = 1.5405\text{\AA}$

The optical response of annealed CdS films was also studied and is shown below.

The bandgap energy (established as the minima of $d\varepsilon_2/dE$) was reduced by approximately 0.1 eV in the twice heat treated case. Similar results were obtained in previous work by A. E. Rakhshani et al. [17]. Rakhshani, attributes the lower bandgap of

annealed CdS to grain-related extended states and a relaxation of the lattice strain which improves the mobility-lifetime product of carriers. Rakhshani also found that this strain is inversely related to the film thickness but only measured CdS films deposited on Soda-Lime glass. Other studies of CdS optical properties [14, 15, 16, 17] also use spectroscopic ellipsometry to measure CdS but only on glass substrates. This lack of substrate variation motivated an analysis of CBD CdS on Cu(In,Ga)Se₂.

Using the optical data obtained for CdS deposited on Mo/7059, a model was built for CdS on accurately well characterized etched and peeled Cu(In,Ga)Se₂ substrates. The CBD recipe used to deposit CdS includes an initial 1 minute ammonia etch which helped eliminate any interface oxide layers [32]. The first fit iteration was used just to fit the thickness of the CdS film and thus the fixed optical constants were not affected by inaccuracies of the substrate. Next, this thickness was held fixed and a point-by-point fit was used to tweak the general oscillator parameters. In further iterations, the thickness of the Cu(In,Ga)Se₂ and CdS layers were allowed to adjust slightly which improved the agreement between point-by-point data and the general oscillator data (shown in Figure 5.12). A 50/50 EMA layer known as an intermix layer was used to model the slightly rough CdS/Cu(In,Ga)Se₂ interface. The thickness of this layer fit to 50-100Å which is expected from AFM measurements on the Cu(In,Ga)Se₂ surface.

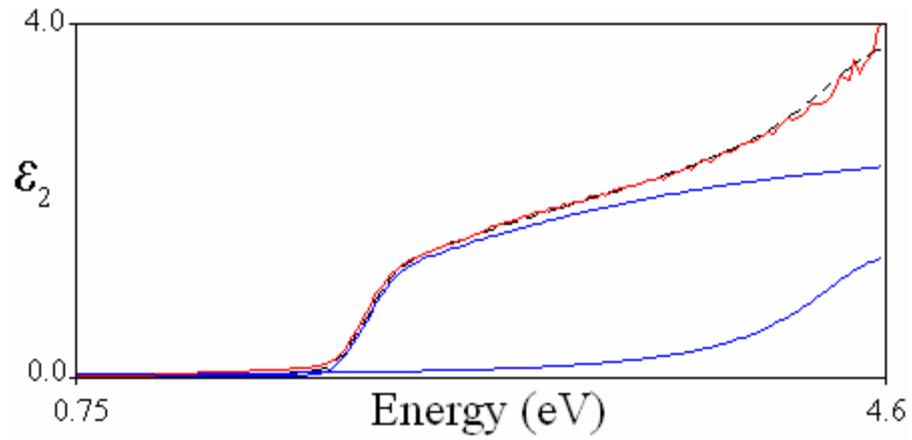


Figure 5.12: Dielectric constant of CdS modeled using two general oscillators. Linear summation of these two oscillators (dotted line) is in good agreement with the point-by-point data (solid line).

Final MSE values obtained using this approach were only slightly higher than the original MSE values of the modeled Cu(In,Ga)Se₂ samples indicating a very good fit of the CdS layer. Optical constants for CdS samples prepared under a variety of conditions are shown in Figure 5.13.

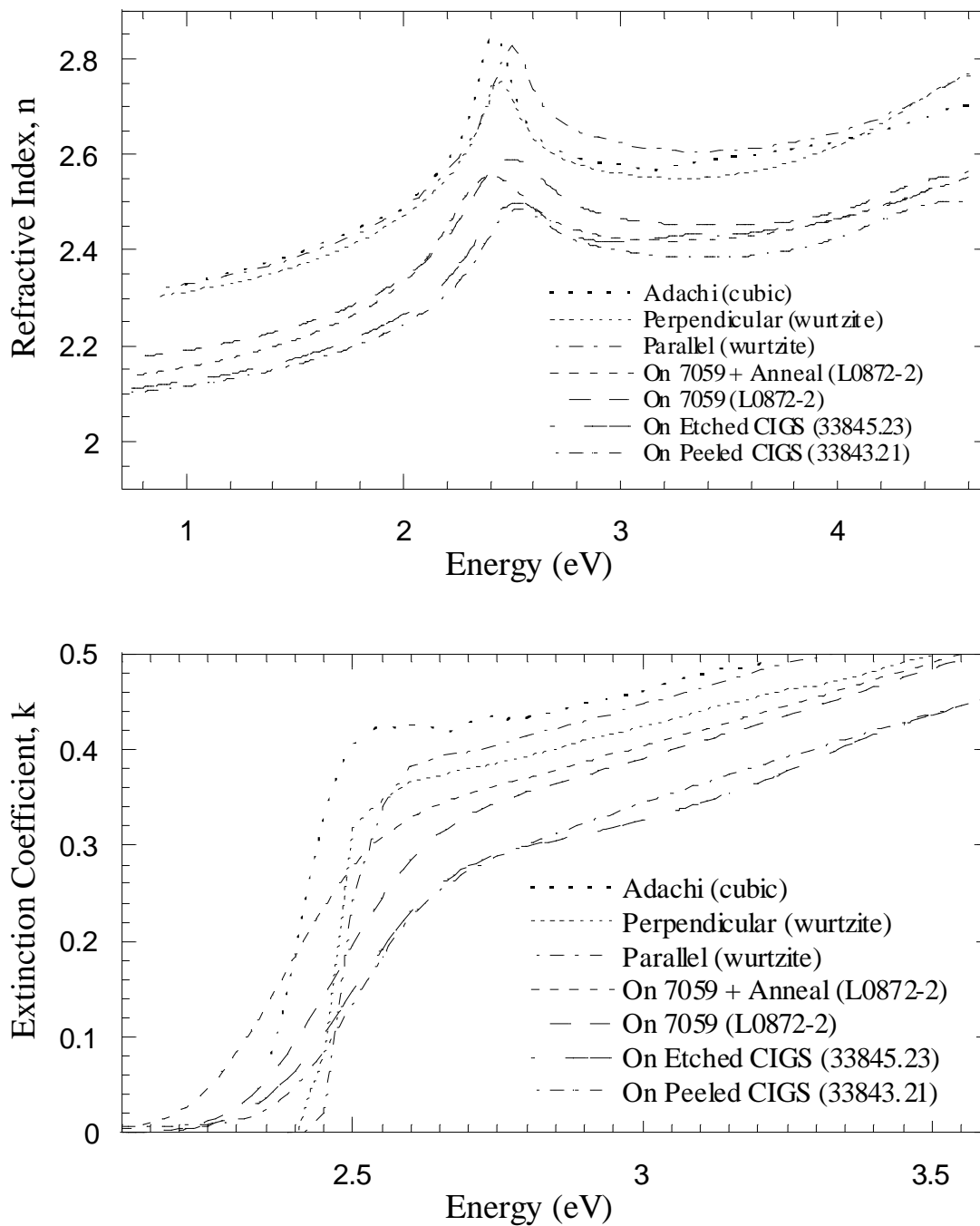


Figure 5.13: Optical constants of CBD CdS and data from literature [38]. Extinction coefficients are shown over a narrowed range to resolve bandgap behavior more clearly. The annealed sample is HT 2 from Figure 5.11. The 7059 lines represent CdS deposited on a Mo/7059 surface.

The data label “Adachi (cubic)”, “Perpendicular (wurtzite)”, and “Parallel (wurtzite)” were measured by Adachi [38] on bulk single CdS crystals. Although the films grown for this work are of the anisotropic wurtzite phase, the films are polycrystalline with randomly orientated grains and assumed to be effectively isotropic. The differences between the optical constants of the CBD CdS films and the Adachi data are significant. The values for the optical constants modeled in this work are lower than those from [38] and also appear less sharp. This difference most likely due to the poorer crystallinity of the CBD grown films as opposed to Adachi’s bulk single crystals. Annealing the films did increase the values of the optical constants in the bandgap region but did not produce the sharp transitions of Adachi’s data. Further annealing of the samples may have produced sharper transitions but the difference could also be indicative of strain in the thin films. A third explanation for this difference should also be noted. Gradual transitions and lower values of the optical constants can sometimes be indicative of slight inaccuracies in the optical model or poor sample preparation causing surface contamination or surface layers. Unfortunately this discrepancy was only discovered when reexamining the data and it was not possible to investigate the matter further. However, the measured CdS films are still comparable to one another and their relative response will be evaluated. It should also be noted that the differences shown between CdS deposited on etched and peeled Cu(In,Ga)Se₂ samples were not obtained repeatedly because of consistency problems modeling etched samples. The fit for CdS on a peeled Cu(In,Ga)Se₂ generally reached a lower MSE and thus these optical data are likely more accurate.

Chapter 6

CONCLUSIONS AND FUTURE WORK

6.1 Conclusion

6.1.1 Mo

The optical response of Mo sputtered on Soda-Lime and 7059 were measured and compared with tabulated data from literature [5]. The optical constants were obtained directly by estimating a roughness from AFM measurements and using this value to fix the roughness EMA layer of the model. The differences in n and k values between Soda-Lime and 7059 samples were not likely due to epitaxial effects because the probing light only penetrated a small fraction of this metal film. Instead, the differences were most likely due to the diffusion of Na into the Mo film of Soda-Lime samples.

6.1.2 MoSe₂

The very thin MoSe₂ layer was modeled by first obtaining optical constants for a selenized Mo sample. Using the optical data from this thicker film, the thickness of the MoSe₂ layer for peeled films could be determined and, after successive fitting iterations, the optical constants were established as well. The n and k values of the peeled MoSe₂ films differed substantially from the selenized sample. These differences, while

significant in a relative sense, had little effect when modeling samples with Cu(In,Ga)Se₂ films. This is because the high absorption and thickness of Cu(In,Ga)Se₂ resulted in the MoSe₂ layer being optical insignificant.

6.1.3 Cu(In,Ga)Se₂

An alternative approach to measuring the optical constants of Cu(In,Ga)Se₂ films was established with the use of chemical Br and KCN etches. Using the previously obtained data on Mo and MoSe₂ layers, a three layer optical model was used to model the n and k values. Optical data obtained with this approach was compared with data measure on peeled samples. However, etched samples yielded slightly poorer fits, particularly near the bandgap, possibly due to a slightly higher surface roughness. Thus a reliable and consistent comparison of the optical constants between peeled and etched samples could not be made.

6.1.4 CdS

CBD CdS layers were analyzed on a variety of surfaces to compare substrate effects. The optical constants of CdS deposited on peeled and etched Cu(In,Ga)Se₂ surfaces were in good agreement. Additionally, the CdS films deposited on Cu(In,Ga)Se₂ surfaces had a bandgap approximately 0.1 eV higher than CdS films deposited on glass. The bandgap of CdS films on glass showed a 0.1eV reduction in the bandgap after annealing. Rakhshani et al. [17] suggests this reduction is due to strain relaxation and thus the higher bandgap of CdS films on Cu(In,Ga)Se₂ could be attributed to increased

lattice strain. Comparisons between the optical constants of the CBD CdS films and the Adachi data [38] is difficult because the transitions modeled in this work are much less sharp and thus parameters such as $d\epsilon_2/dE$ may be inaccurate. Further study is required to determine if these discrepancies are due to actual differences between bulk CdS crystals and thin films or merely a result of systematic errors such as unaccounted surface layers.

6.1.5 Ellipsometry

Variable angle spectroscopic ellipsometry is a precise analysis technique for studying how the optical response of materials differs between thin films and bulk material. With careful modeling techniques, VASE measurements can also be used to study films prepared in layer structures offering the possibility of analyzing the optical properties of a manufactured device. However, care must be taken when interpreting the results of analyzed devices. Very thin surface or interface layers can significantly affect the measured values of Ψ and Δ . Often these layers will prevent successive modeling of the sample but a more difficult problem arises when the effect of the unknown layers is slight. In this case, the slight effect of the interface or surface layer can be compensated for by the one or more of the layers in the optical model resulting in a model that produces the “effective” optical constants rather than the true response of the films. For this reason, VASE measurements are best performed in conjunction with other analysis techniques.

6.2 Future Work

The focus of this work was the development of methods to study the layered structure of Cu(In,Ga)Se₂ films and analysis of how the optical properties of materials changed under various preparations techniques. These variations in optical response were significant in the case of the MoSe₂ and CdS layers. However, the physical basis for this variation with sample preparation was not explored. In order to successfully correlate the optical functions of a film with band structure models or phase diagrams, greater diversity of sample preparation techniques, more extensive non-VASE analysis, and a better theoretical understanding would be required.

Additionally, at least two specific aspects of this work merit further study. The first is the confirmation or rejection of differences in the optical constants between the Cu(In,Ga)Se₂ layer of peeled and etched samples. If this difference exist, it is likely to be small but could yield information regarding the MoSe₂/Cu(In,Ga)Se₂ interface. The second area is regarding the differences in optical constants of CdS layers with different preparation techniques. Currently, a chemical surface deposition (CSD) is a promising alternative to the material intensive CBD process. A detailed study of the optical constants of CSD prepared films on Cu(In,Ga)Se₂ substrates could help in understanding the device performance differences seen between these two deposition techniques.

BIBLIOGRAPHY

- 1 Marketbuzz 2005: annual world solar photovoltaic (PV) market report (2005).
- 2 C. Whitaker and M. Real, *The impact of efficiency on area-related system costs*, Progress in Photovoltaics: Research and Applications **7**, 199 (1999).
- 3 M. Rogol and S. Doi, *When will the good times end?*, Photon International, January, pp 36-40 (2005).
- 4 W. N. Shafarman and L. Stolt, in Handbook of Photovoltaic Science and Engineering, Ch. 13, John Wiley & Sons, 2003.
- 5 E. D. Palik, Handbook of Optical Constants of Solids. Academic Press, New York, 1985.
- 6 K. Vedam, *Spectroscopic ellipsometry: a historical overview*, Thin Solid Films **313-314**, 1 (1998).
- 7 H. R. Philipp and E. A. Taft, *Optical Constants of Germanium in the Region 1 to 10 eV*, Physical Review **113**, 1002 (1959).
- 8 D. E. Aspnes and A. A. Stunda *High Precision Scanning Ellipsometer*, Applied Optics **14**, 220 (1975).
- 9 T. Kawashima, S. Adachi, H. Miyake, and K. Sugiyama, *Optical constants of CuGaSe₂ and CuInSe₂*, Journal of Applied Physics **84**, 5202 (1998).
- 10 M. I. Alonso, K. Wakita, J. Pascual, M. Garriga, and N. Yamamoto, *Optical functions and electronic structure of CuInSe₂, CuGaSe₂, CuInS₂, and CuGaS₂*, Physical Review B **63**, 075203 (2001).
- 11 M. I. Alonso, M. Garriga, C. A. Durante Rincon, E. Hernandez, and M. Leon, *Optical functions of chalcopyrite CuGa_xIn_{1-x}Se₂ alloys*, Applied Physics A **74**, 659 (2002).

- 12 A.M. Hermann, C. Gonzales, P.A. Ramakrishnan, D. Balzar, N. Popa, P. Rice, C. H. Marshall, J. N. Hilfiker, T. Tiwald, P. J. Sebastian, M. E. Calixto, and R. N. Bahattacharya, *Fundamental studies of large area Cu(In,Ga)Se₂ films for high efficiency solar cells*, Solar Energy Materials & Solar Cells **70**, 345 (2001).
- 13 P. D. Paulson, R. W. Birkmire, and W. N. Shafarman, *Optical characterization of CuIn_{1-x}GaxSe₂ alloy thin films by spectroscopic ellipsometry*, Journal of Applied Physics **94**, 879 (2003).
- 14 S. Ninomiya and S. Adachi, *Optical properties of wurtzite CdS*, Journal of Applied Physics **78**, 1183 (1995).
- 15 K. Senthil, D. Mangalaraj, Sa. K. Narayandass, S. Adachi, *Optical constants of vacuum-evaporated cadmium sulphide thin films measurement by spectroscopic ellipsometry*, Materials Science and Engineering **B78**, 53 (2000).
- 16 S. Mathew, P. S. Mukerjee, and K. P. Vijayakumar, *Optical and surface properties of spray-pyrolysed CdS thin films*, Thin Solid Films **254**, 278 (1995).
- 17 A. E. Rakhshani and A. S. Al-Azab, *Characterization of CdS films prepared by chemical-bath deposition*, Journal of Physics: Condensed Matter **12**, 8745 (2000).
- 18 Software Manual. Guide to Using WVASE32. J.A. Woollam Co., 1997.
- 19 M. Fox. Optical Properties of Solids. Oxford University Press Inc., New York, 2001.
- 20 H. G. Tompkins, W. A. McGahan. Spectroscopic Ellipsometry and Reflectometry: A User's Guide. John Wiley & Sons, New York, 1999.
- 21 J. A. Woollam. V.A.S.E. Product Brochure. Lincoln Nebraska. <http://www.jawoollam.com/pdf/vase.pdf>.
- 22 F. A. Jenkins and H. E. White. Fundamentals of Optics. McGraw-Hill Inc., New York, 1976.
- 23 P. D. Paulson and S. S. Hegedus, *Accurate determination of optical constants of textured SnO₂ using low incidence angle spectroscopic ellipsometry*, Journal of Applied Physics **96**, 5469 (2004).
- 24 J. A. Woollam. Wiley Encyclopedia of Electrical and Electronics Engineering: Ellipsometry, Variable Angle Spectroscopic. John Wiley & Sons, New York, 2000.

- 25 D. E. Aspnes and J. B. Theeten, *Investigation of effective-medium models of microscopic surface roughness by spectroscopic ellipsometry*, Physical Review B **20**, 3292 (1979).
- 26 G. E. Jellison, Jr., *Use of the biased estimator in the interpretation of spectroscopic ellipsometry data*, Applied Optics **30**, 3354 (1991).
- 27 W. H. Press, B. P. Flannery, S. A. Teukolsky, and W. T. Vetterling, Numerical Recipes. Cambridge University Press, Cambridge, 1998.
- 28 W. N. Shafarman, R. Klenk, and B. E. McCandless, *Device and material characterization of Cu(InGa)Se₂ solar cells with increasing band gap*, Journal of Applied Physics **79**, 7324 (1996).
- 29 W. N. Shafarman and J. Zhu, *Effect of substrate temperature and deposition profile on evaporated Cu(InGa)Se₂ films and devices*, Thin Solid Films **361**, 473 (2000).
- 30 S. Nishiwaki, N. Kohara, T. Negami, and T. Wada, *MoSe₂ layer formation at Cu(In,Ga)Se₂/Mo Interfaces in high efficiency Cu(In_{1-x}Ga_x)Se₂ solar cells*, Japanese Journal of Applied Physics **37**, L71 (1998).
- 31 P. D. Paulson, S. H. Stephens, and W. N. Shafarman, *Analysis of Cu(In,Ga)Se₂ Alloy Film Optical Properties and the Effect of Cu Off-Stoichiometry*, Materials Research Society Symposium Proceedings **865**, (2005).
- 32 J. Kessler et al., Tech. Digest, PVSEC **6**, 1005 (1992).
- 33 R. W. Birkmire and B. E. McCandless, *Specular CuInSe₂ films for solar cells*, Applied Physics Letters **53**, 140 (1988).
- 34 B. Canava, J. F. Guillemoles, J. Vigneron, D. Lincot, and A. Etcheberry, *Chemical elaboration of well defined Cu(In,Ga)Se₂ surfaces after aqueous oxidation etching*, Journal of Physics and Chemistry of Solids **64**, 1791 (2003).
- 35 B. Canava, J. Vigneron, A. Etcheberry, J. F. Guillemoles, and D. Lincot, *High resolution XPS studies of Se chemistry of a Cu(In,Ga)Se₂ surface*, Applied Surface Science **202**, 8 (2002).
- 36 D. Abou-Ras, G. Kostorz, D. Bremaud, M. Kalin, F. V. Kurdesau, A. N. Tiwari, M. Dobeli, *Formation and characterization of MoSe₂ for Cu(In,Ga)Se₂ based solar cells*, Thin Solid Films **480-481**, 433 (2005).

- 37 B. Tell and P. M. Bridenbaugh, *Aspects of the band structure of CuGaS₂ and CuGaSe₂*, Physical Review B **12**, 3330 (1975).
- 38 S. Adachi. Optical Constants of Crystalline and Amorphous Semiconductors. Kluwer Academic Publishers, Boston, 1999.